

Integrated Balanced and Staggered Routing in Autonomous Mobility-on-Demand Systems

Antonio Coppola¹, Gerhard Hiermann², Dario Paccagnan³, Michel Gendreau⁴, and Maximilian Schiffer^{1,5}

¹School of Management, Technical University of Munich, Germany

`antonio.coppola@tum.de`

²Institute of Production and Logistics Management, Johannes Kepler University Linz, Austria

`gerhard.hiermann@jku.at`

³Department of Computing, Imperial College London, U.K.

`d.paccagnan@imperial.ac.uk`

⁴Department of Mathematical and Industrial Engineering, Polytechnique Montréal, Canada

`michel.gendreau@polymtl.ca`

⁵Munich Data Science Institute, Technical University of Munich, Germany

`schiffer@tum.de`

Abstract

Autonomous mobility-on-demand (AMoD) systems — centrally coordinated fleets of self-driving vehicles — offer a promising alternative to traditional ride-hailing by improving traffic flow and reducing operating costs. Centralized control in AMoD systems enables two complementary routing strategies: balanced routing, which distributes traffic across alternative routes to ease congestion, and staggered routing, which delays departures to smooth peak demand over time. In this work, we introduce a unified framework that jointly optimizes both route choices and departure times to minimize system travel times. We formulate the problem as an optimization model and show that our congestion model yields an unbiased estimate of travel times derived from a discretized version of Vickrey’s bottleneck model. To solve large-scale instances, we develop a custom metaheuristic based on a large neighborhood search framework. To assess our method, we conduct a case study on the Manhattan street network using real-world taxi data. In a setting with exclusively centrally controlled AMoD vehicles, our approach reduces total traffic delay by up to 25% and mitigates network congestion by up to 35% compared to selfish routing. We also consider mixed-traffic settings with both AMoD and conventional vehicles, comparing a welfare-oriented operator that minimizes total system travel time with a profit-oriented one that optimizes only the fleet’s travel time. Independent of the operator’s objective, the analysis reveals a win–win outcome: across all control levels, both autonomous and non-autonomous traffic benefit from the implementation of balancing and staggering strategies.

Keywords: autonomous mobility-on-demand; balanced routing; staggered routing

1. Introduction

The ride-hailing market has recently experienced substantial growth, fueled by evolving consumer preferences and technological innovations. Projections estimate that by 2028, ride-booking platforms will serve nearly 100 million users, driving the U.S. market to a value of approximately \$55 billion (Statista 2024).

While ride-hailing services offer convenient transportation options, they have been criticized for exacerbating urban congestion (Diao et al. 2021), primarily due to uncoordinated operations (Kondor et al. 2022) and drivers favoring personal route choices (Zanardi et al. 2023), which result in suboptimal travel patterns and overloaded networks. This inefficiency carries a dual cost: from a societal standpoint, it worsens congestion and its externalities, including prolonged delays, air and noise pollution, and broader public health impacts; from the operator’s standpoint, it drives up operational costs through increased travel time, fuel use, and vehicle underutilization.

Autonomous mobility-on-demand (AMoD) systems, centrally controlled fleets of self-driving vehicles offering door-to-door mobility solutions (Pavone 2015), promise to overcome these limitations. Their central governance enables the coordination of vehicle flow in response to travel demand and traffic conditions, mitigating the inefficiencies associated with self-interested, uncoordinated fleets of human-driven vehicles. However, without effective routing policies, AMoD systems risk replicating the issues observed in traditional ride-hailing services, potentially further straining the street network (Oh et al. 2020). To address congestion and enhance operational efficiency, AMoD routing policies can employ two main coordination strategies: balanced and staggered routing. Balanced routing distributes AMoD flow across alternative road segments to alleviate congestion on popular routes and smooth overall traffic flow. Staggered routing complements this approach by strategically delaying vehicle departures to spread demand more evenly over time, alleviating temporal imbalances in network utilization.

Although complementary, these operational strategies lack a unified framework for integrated implementation in AMoD systems. On one hand, most existing studies that address AMoD routing under congestion rely on static models (cf. Zardini et al. 2022), which are well-suited for long-term planning but fall short in supporting AMoD operations for two key reasons: first, they cannot capture the real-time nature of fleet management, which must continuously adapt to evolving travel demand; second, they cannot accommodate departure time assignments, which require explicit temporal modeling. On the other hand, previous work on optimal staggering of AMoD departures lacks a routing control layer that leverages the additional travel time reductions enabled by staggering, thus treating route and departure time assignments in *isolation*.

In contrast, an *integrated* approach combines these strategies by moving the departure time decision to an earlier control stage. This shift influences route selection and can potentially outperform balanced and staggered routing methods when applied in isolation. However, this integrated optimization introduces additional combinatorial complexity and challenges the tractability of existing solution approaches. Against this background, we explore the untapped potential of integrating balanced and staggered routing strategies to coordinate autonomous fleets more efficiently under high

travel demand. It introduces scalable algorithmic solutions to jointly optimize route assignment and departure timing, addressing the computational and operational complexity of large-scale, dynamic fleet coordination while accounting for congestion.

1.1. Contribution

This paper makes the following contributions. First, we formalize the problem of minimizing travel time in a network operated by a AMoD system using an integrated approach that combines balanced and staggered routing. Second, we formally show that the congestion model employed serves as an unbiased estimator of travel times under a discretized version of Vickrey’s bottleneck model — a well-established framework in dynamic traffic assignment. Third, given that the staggered routing problem—optimizing AMoD departure times along fixed routes—is already NP-hard (Coppola et al. 2025), we develop a scalable metaheuristic based on a large neighborhood search (LNS) framework to solve the more general problem of jointly optimizing routes and departure times. We relax the assumption of piecewise-linear delay constraints and enable our algorithm to handle any convex, non-decreasing delay function. Fourth, we go beyond prior implicit representations of baseload traffic in the staggered routing literature by explicitly modeling a realistic number of trips, approximating real-world congestion conditions. Existing approaches typically rely on a mixed integer linear program (MILP) formulation tightened through trip time windows; however, the large number of resulting constraints limits the number of trips that can be explicitly tracked. To circumvent this, prior work approximates baseload traffic by imposing arc capacity limits instead of modeling individual trips — a limitation we overcome by no longer utilizing a MILP formulation. Finally, we conduct a numerical study using real-world data from Manhattan, New York City, to examine the trade-offs between adjusting vehicle routes and departure times to minimize travel times and study network congestion. Our case study initially assumes the AMoD operator has full traffic control, showing that our algorithmic solutions reduce fleet delays by up to 25% and congestion delays by up to 35% compared to a selfish baseline. We then transition to a mixed-traffic setting, where AMoD vehicles serve only a fraction of the demand. This allows us to examine how varying the level of control affects overall network performance. In both welfare- and profit-oriented settings, centralized balanced and staggered routing consistently produce a win-win outcome, reducing travel times for both AMoD and non-AMoD traffic across all scenarios. Notably, controlling just 10% of the system’s vehicles already achieves 25% of the maximum delay reduction, while 50% control yields 75%, with further gains becoming more marginal.

2. Related literature

Our work builds upon previous research aimed at mitigating congestion through strategic routing and timing of traffic. First, adopting a theoretical perspective, we highlight the intersections of this work with the field of dynamic traffic assignment (DTA). Second, from an applicative perspective, we focus on control and operational strategies for AMoD systems.

Overview of DTA models The primary objective of traffic assignment is to model vehicular movement patterns based on predefined behavioral rules. A DTA model typically consists of a route and/or departure choice model combined with a traffic congestion model, so we review both components in sequence. Based on the available route and departure time choices, DTA models fall into one of three main categories: (1) pure departure time choice models (see, e.g., Vickrey 1969, Hendrickson & Kocur 1981, Lindsey et al. 2012), (2) pure route choice models (see, e.g., Mounce & Carey 2011, Carey & Watling 2012, Long et al. 2013, Levin 2017), and (3) simultaneous route and departure time choice (SRDTC) models (see, e.g., Jauffred & Bernstein 1996, Ran et al. 1996, Ziliaskopoulos & Rao 1999, Huang & Lam 2002, Han et al. 2013, Jalota et al. 2023).

Focusing on SRDTC models, which are closest in nature to our work, route and departure time choices typically follow either the dynamic user optimal principle—where travelers select routes and departure times to minimize their own travel costs (Nie 2010, Friesz et al. 2011, Ukkusuri et al. 2012)—or the dynamic system optimal principle, which seeks to minimize total system-wide travel cost (Long et al. 2018). Efforts to bridge the gap between user equilibrium and system optimality in SRDTC models include tolling schemes (Arnott et al. 1990, Yang & Meng 1998, Liu & Nie 2011), demand management and route guidance systems (Makridis et al. 2024, Menelaou et al. 2021), and signal control (Hu & Mahmassani 1997). Despite these efforts, research on achieving dynamic system optimality or dynamic fleet optimality (Battifarano & Qian 2023) through centralized control of departures and routes remains limited.

A complete DTA model combines travelers’ behavioral choices with a congestion model that captures how traffic evolves over time along routes connecting origin-destination pairs. Commonly adopted congestion models include extensions of Vickrey’s bottleneck model, which represent traffic formation and dissipation as a vertical queue at the bottleneck entrance, offering analytically tractable formulations (Li et al. 2020), and cell transmission models, which can capture complex dynamics such as spillback effects (Adacher & Tiriolo 2018). However, applying these models to large-scale networks remains computationally demanding (Ziliaskopoulos et al. 2004). To address this, researchers have proposed macroscopic fundamental diagram-based models as aggregated tools for analyzing large-scale traffic behavior (Aghamohammadi & Laval 2020). In this work, we introduce a discretized congestion model inspired by Vickrey’s bottleneck framework, enabling explicit vehicle-level routing and timing while preserving computational tractability.

AMoD control & operations Most mesoscopic and macroscopic studies examining the impact of congestion in AMoD systems focus on strategic control settings, optimizing the routes of customer-carrying and rebalancing trips under steady-state conditions (see, e.g., Rossi et al. 2018, 2020, Estandia et al. 2021, Salazar et al. 2019, Bahrami & Roorda 2020, Bang & Malikopoulos 2022). While these approaches are valuable for long-term evaluation, they overlook the dynamic nature of AMoD operations, limiting their applicability to our setting.

In contrast, research that considers the dynamic aspects of AMoD operations, including studies on vehicle dispatching (see, e.g., Zhang et al. 2017, Xu et al. 2018, Li et al. 2019, Tang et al. 2019, Zhou

et al. 2019, Liang et al. 2021, Sadeghi Eshkevari et al. 2022, Enders et al. 2023), joint dispatching and rebalancing (see, e.g., Tsao et al. 2018, Jungel et al. 2023), request pooling (see, e.g., Alonso-Mora et al. 2017, Tsao et al. 2019), and fleet rebalancing (see, e.g., Liu & Samaranayake 2022, Iglesias et al. 2018, Jiao et al. 2021, Gammelli et al. 2021, Skordilis et al. 2021) rarely explicitly model congestion, as many rely on precise forecasts or deterministic assumptions for travel times.

In this work, we develop a scalable framework that explicitly models congestion and supports balanced and staggered routing for AMoD systems. Our model enables dynamic assignment of routes and departure times at the vehicle level, using a congestion model inspired by Vickrey’s bottleneck formulation to provide a tractable representation of traffic dynamics.

2.1. Roadmap

The remainder of this paper is organized as follows. Section 3 introduces the problem setting for the integrated balanced and staggered routing problem and shows the relation between our congestion model and Vickrey’s bottleneck model. Section 4 describes our metaheuristic algorithm developed to solve real-world instances. In Section 5, we outline our experimental design, and in Section 6, we present the results from our numerical study. Finally, Section 7 concludes the paper with remarks and future research directions.

3. Problem setting

We consider an AMoD operator tasked with coordinating a fleet of autonomous vehicles to serve a given set of trips within a fixed planning horizon. We focus on an offline setting in which the operator has full knowledge of all trip requests in advance. Each trip utilizes a single vehicle and can represent either on-duty activities (e.g., customer delivery) or off-duty activities (e.g., rebalancing). Our objective is to minimize total travel time by jointly optimizing route selection and trip departure times. This involves balancing trips across alternative (potentially longer in distance) routes and staggering departures beyond their originally requested times to prevent congestion and improve fleet efficiency.

We model the road network within which the fleet operates as a directed graph $\mathcal{G} = (\mathcal{V}, \mathcal{A})$, where the nodes \mathcal{V} represent trip origins, destinations, and road intersections, and the arcs \mathcal{A} correspond to road segments connecting these nodes. We consider a set of trips \mathcal{R} , each traveling between two distinct network nodes. Let a quadruple $(\mathcal{P}^r, e^r, \ell^r, \bar{\sigma}^r)$ define a trip $r \in \mathcal{R}$, with $\mathcal{P}^r = \{p_1^r \dots p_k^r\}$ denoting the alternative k routes – sequences of network arcs – that the vehicle can travel, e^r being the earliest departure from the trip’s origin, ℓ^r being the latest feasible arrival at the destination, and $\bar{\sigma}^r$ being the maximum staggering time applicable to a trip’s departure. A trip r traversing arc a experiences a travel time $\tau_a^r(f_a^r)$, which consists of two components: the free-flow travel time τ_a and a congestion-induced delay $d(f_a^r)$. The delay depends on the number of trips f_a^r present on arc

a at the time r begins its traversal:

$$\tau_a^r(f_a^r) = \tau_a + d(f_a^r), \quad (3.1)$$

where $d(f_a^r)$ is a convex, non-decreasing function of flow. A tuple $\pi = (p, s)$ defines a solution to this problem, where p and s denote the route and departure time assigned to each trip r , respectively. As we assume that vehicles do not idle once a trip has started, this information is sufficient to determine the travel time along each selected route and, consequently, the arrival time for every trip. We require a solution π to satisfy the following constraints, which we collect in the feasible set Π :

- i) The route p^r assigned to each trip r must belong to \mathcal{P}^r .
- ii) The start time s^r of each trip r must occur between e^r and $e^r + \bar{\sigma}^r$.
- iii) The combination of start times and routes in π must ensure that the arrival at the destination of each trip r occurs before ℓ^r .

In this setting, we seek for a solution $\pi^* \in \Pi$ that minimizes the total fleet travel time, defined as the sum of travel times incurred by each trip across the arcs of its assigned route:

$$\min_{\pi \in \Pi} Z^\pi = \sum_{p^r \in \pi} \sum_{a \in p^r} \tau_a^r(\pi), \quad (3.2)$$

where, with slight abuse of notation, we make explicit that the travel time τ_a^r experienced by trip r on arc a depends on all route and departure time assignments.

Discussion A few comments on our modeling approach are in order. First, we assume that only AMoD trips traverse the network, meaning the operator has full control over all trips in \mathcal{R} to keep this basic problem setting concise. To extend the model to include background traffic, one can designate a subset of trips with routes and departure times not subject to optimization. This extension also enables the definition of two distinct objective functions: one that minimizes total system travel time, and another that minimizes only the travel time of the controlled trips. We present such an extended formulation in Section 6.

Second, incorporating route choice enhances behavioral realism beyond pure staggering models but increases computational complexity. To ensure scalability, we precompute a set of alternative routes—an approach aligned with route-based methods commonly used in dynamic traffic assignment (cf. Lo & Szeto 2002). As detailed in Sections 4 and 5, we design these routes to support effective balancing while preserving realistic travel patterns within the network.

Finally, although stochastic demand modeling would better capture real-world uncertainty, we assume full knowledge of demand at the central controller. This assumption aligns with the exploratory focus of our study, which aims to quantify the *potential* benefits of integrated balanced and staggered routing in AMoD systems and to provide an upper bound on travel time reductions that can serve as a benchmark for online methods.

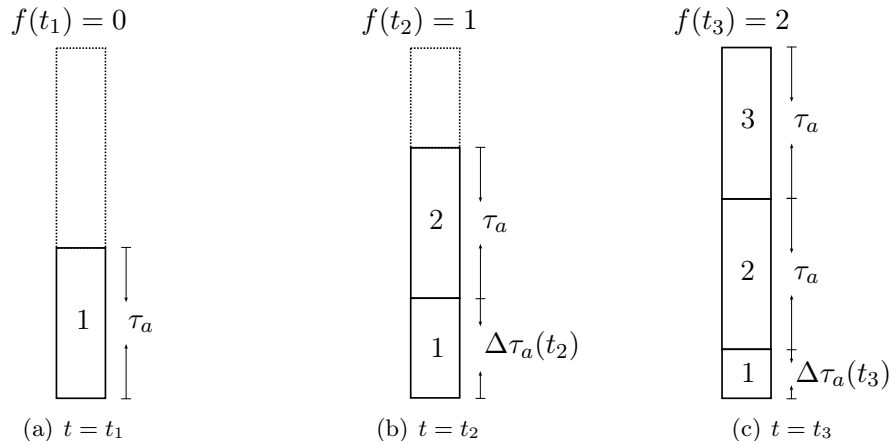


Figure 1: Evolution of a bottleneck at three distinct time steps, t_1 , t_2 , and t_3 , corresponding to the departure times of three distinct trips.

Relation to the discretized Vickrey's bottleneck model Consider an arc with nominal travel time τ_a . Let $f(t)$ denote the flow on this arc at time t , and let $\tau(t)$ represent the corresponding travel time, defined as:

$$\tau(t) = \tau_a + (\phi \cdot \tau_a) f(t), \quad (3.3)$$

where $\phi \in (0, 1]$ is a scalar parameter that quantifies the sensitivity of travel time to congestion. We claim that, under Poisson arrivals, there exists a unique choice of ϕ that renders (3.3) an unbiased estimator of travel times in the discretized Vickrey bottleneck model (cf. Otsubo & Rapoport 2008). To establish this claim, we first review the key features of the discretized Vickrey bottleneck model and show that, under a stable Poisson arrival process, it is equivalent to an M/D/1 queueing system (cf. Thomopoulos 2012). We then map our congestion model onto this queueing framework, allowing us to identify the unique value of ϕ that ensures an unbiased estimation of travel times.

Consider a finite set of trips traveling along a bottleneck road that connects a common origin to a common destination. The bottleneck has a nominal travel time τ_a and a capacity that restricts the number of vehicles simultaneously traversing it. We assume unit capacity, such that at most one trip can pass through the bottleneck at a time, while the remaining trips must wait in a first-in first-out (FIFO) queue. Figure 1 schematizes the evolution of the system. The travel time for a trip departing at time t follows:

$$\tau^V(t) = \begin{cases} \tau_a, & \text{if } f(t) = 0 \\ \Delta\tau_a(t) + f(t) \cdot \tau_a, & \text{otherwise} \end{cases} \quad (3.4)$$

where $\Delta\tau_a(t)$ represents the remaining time for the traveling trip to leave the bottleneck. Assume Poisson arrivals at the bottleneck with rate $\lambda \leq \tau_a^{-1}$. In this setting, (3.4) functions as a stable

M/D/1 queueing system since the service time is constant and equal to τ_a . Let $\rho = \lambda \cdot \tau_a$ denote the traffic intensity of the system. The expected travel time at the bottleneck then follows:

$$\mathbb{E}[\tau^V(t)] = \tau_a + \frac{\tau_a \cdot \rho}{2(1 - \rho)}. \quad (3.5)$$

We are now ready to show that, with an appropriate choice of parameters, Equation (3.3) yields expected travel times that match those of the discretized Vickrey bottleneck model in Equation (3.5). We refer the reader to Appendix A for the proof.

Theorem 1. Consider an arc with nominal travel time τ_a , where arrivals follow a Poisson process with rate $\lambda \leq \tau_a^{-1}$. Let the arc travel time be defined by Equation (3.3). Then, by setting $\phi = (2 - \rho)^{-1}$, the expected travel time under Equation (3.3) coincides with the expected travel time given by Equation (3.5).

This theorem offers the following interpretation. When $\rho = 1$, the system operates at capacity, and the average traversal time $\Delta\tau_a$ equals τ_a . In this case, setting $\phi = 1$ reproduces this behavior, ensuring that delay increases by τ_a per trip ahead. When $\rho < 1$, the average $\Delta\tau_a$ falls below τ_a , so setting $\phi = (2 - \rho)^{-1}$ appropriately compensates for the reduced average delay.

4. Methodology

In this section, we present our methodology for solving large instances of Problem (3.2). Section 4.1 outlines the approach used to design alternative routes for balancing assignments. Section 4.2 introduces a mathematical formulation of the problem, including the notation and constraints that define feasible solutions. While this formulation serves as a valuable *descriptive* tool, it is computationally impractical for large-scale instances. Therefore, in Section 4.3, we propose a custom metaheuristic based on a LNS framework, designed to efficiently generate high-quality solutions at scale.

4.1. Alternative route design

Designing effective route alternatives is central to traffic balancing and congestion mitigation, yet it poses a critical trade-off between spatial diversity and route plausibility.

Solving a k -shortest path problem tends to produce highly overlapping routes, funneling demand onto a few shared arcs. This results in unrealistically high congestion and limits the AMoD controller’s ability to distribute traffic effectively. In contrast, k -disjoint shortest paths enhance route diversity but often span significantly greater distances than the shortest route. Consequently, trips follow implausible detours that distort congestion estimates, and AMoD controllers frequently reject them due to tight arrival time constraints.

To balance these limitations, we solve a k -shortest paths with limited overlap (kSPwLO) problem for each trip r . Given a desired number of alternative routes k and a similarity threshold $\theta\%$, the goal is to compute a set \mathcal{P}^r of k routes connecting the origin and destination of r , such that all

route pairs are sufficiently dissimilar. Specifically, for all $\{p_i^r, p_j^r\} \in \binom{\mathcal{P}^r}{2}$, we require:

$$\text{Sim}(p_i^r, p_j^r) = \frac{\sum_{a \in p_i^r \cap p_j^r} \ell(a)}{\min\{\ell(p_i^r), \ell(p_j^r)\}} \leq \theta,$$

with $p_i^r \cap p_j^r$ denoting shared arcs, and $\ell(\cdot)$ the arc or path length.

To solve the kSPwLO problem efficiently, we adopt the SVP^+ algorithm (Chondrogiannis et al. 2020), a performance-oriented heuristic designed for large-scale networks. SVP^+ restricts the search space to *single-via paths* (Abraham et al. 2013), obtained by concatenating a shortest path from the source to an intermediate node with another shortest path from that node to the target. The algorithm first computes the shortest paths from the source to all nodes and from all nodes to the target. It then evaluates candidate paths formed by combining these partial paths and ranks them by length. As a final step, the algorithm incrementally adds paths to the solution set if they are sufficiently dissimilar from those already selected. Finally, we note that the resulting path sets satisfy the following properties:

- i) they always include the shortest path;
- ii) all selected paths meet the similarity threshold θ ;
- iii) the selected paths are as short as possible within the restricted set.

4.2. Mathematical programming formulation

Our goal is to formulate Problem (3.2) as a mathematical program. We begin by introducing the necessary variables, then formalize the constraints using an indicator function, and finally discuss the linearization of this function and explain why it renders the formulation intractable.

For every trip $r \in \mathcal{R}$, we define the binary variable $y_i^r \in \{0, 1\}$, which takes the value 1 when the i -th route serves trip r and remains 0 otherwise, with $1 \leq i \leq k$. To account for increased travel time due to congestion, we introduce a delay variable d_a^r for each arc appearing in the alternative routes \mathcal{P}^r of trip r . This delay satisfies $d_a^r = d(f_a^r)$, where $d(f_a^r)$ is a convex, non-decreasing function of flow. We also introduce non-negative travel time variables $\tau_a^r \geq 0$ for the same set of arcs and trips. These variables take positive values only on arcs that belong to the selected route and are zero otherwise. To enforce this behavior, together with the objective function minimizing the sum of the travel time variables, we apply the following big-M constraints:

$$\tau_a^r \geq \tau_a + d_a^r - M(1 - y_i^r), \quad \forall r \in \mathcal{R}, i \leq k, a \in p_i^r$$

where M denotes a sufficiently large constant.

To model the temporal progress of each trip along its route, we introduce continuous variables s_a^r and \bar{s}_a^r for each arc in every alternative route, representing the start and completion times of the traversal of arc a by trip r . Finally, we denote \underline{p}_i^r and \bar{p}_i^r as the first and last arcs of route p_i^r , respectively. We formulate the problem as:

$$\min \sum_{r \in \mathcal{R}} \sum_{i \leq k} \sum_{a \in p_i^r} \tau_a^r \quad (4.1a)$$

$$\begin{aligned}
& \text{s.t.} \\
& \sum_{i=1}^k y_i^r = 1, & \forall r \in \mathcal{R} & (4.1b) \\
& d_a^r = d(f_a^r), & \forall r \in \mathcal{R}, i \leq k, a \in p_i^r & (4.1c) \\
& \tau_a^r \geq \tau_a + d_a^r - M(1 - y_i^r), & \forall r \in \mathcal{R}, i \leq k, a \in p_i^r & (4.1d) \\
& f_a^r = \sum_{r' \in \mathcal{R} \setminus \{r\}} \mathbb{I}(\underline{s}_a^{r'} \leq \underline{s}_a^r < \bar{s}_a^{r'}), & \forall r \in \mathcal{R}, i \leq k, a \in p_i^r & (4.1e) \\
& \bar{s}_a^r = \underline{s}_a^r + \tau_a^r, & \forall r \in \mathcal{R}, i \leq k, a \in p_i^r & (4.1f) \\
& e^r \leq \underline{s}_a^r \leq e^r + \bar{\sigma}^r, & \forall r \in \mathcal{R}, i \leq k, a = \bar{p}_i^r & (4.1g) \\
& \bar{s}_a^r \leq \ell^r, & \forall r \in \mathcal{R}, i \leq k, a = \bar{p}_i^r & (4.1h) \\
& \underline{s}_a^r, \bar{s}_a^r, f_a^r, d_a^r, \tau_a^r \geq 0, & \forall r \in \mathcal{R}, i \leq k, a \in p_i^r & (4.1i) \\
& y_i^r \in \{0, 1\}, & \forall r \in \mathcal{R}, i \leq k & (4.1j)
\end{aligned}$$

The objective in (4.1a) minimizes the total travel time of the fleet. Constraint (4.1b) ensures the selection of exactly one route for each trip. Constraints (4.1c)-(4.1d), together with the definitions of the variables d_a^r and τ_a^r in (4.1i), calculate the travel time for trips on the arcs of their selected routes and ensure that travel time is zero for non-selected routes. Constraint (4.1e) determines the number of trips encountered by a trip r upon entering arc a , using the indicator function $\mathbb{I}(\cdot)$. Constraint (4.1f) propagates the departure times of trips along their routes. Constraints (4.1g)-(4.1h) enforce time window restrictions for each trip. Finally, Constraints (4.1i)-(4.1j) define the domains of the decision variables.

Directly solving the formulation presented is impractical due to the presence of the indicator function in (4.1e). To address this, we replace it with an additional set of big-M constraints, obtaining a mixed-integer convex program. For a detailed description of this approach, we refer the reader to Section 3.1 of Coppola et al. (2025), which provides a procedure that applies almost directly to our extended setting. The key distinction in this case lies in the requirement to define a set of big-M constraints for all pairs of trips that may *potentially* traverse a given arc, that is, for trips for which the arc belongs to at least one alternative route. Even under a simple specification of $d(f_a^r)$, such as a linear or piecewise linear function (resulting in a mixed-integer linear program), the number of big-M constraints required for linearization is significantly higher compared to a setting with fixed routes, rendering the formulation computationally intractable. Therefore, rather than attempting to solve this MILP directly, we develop a metaheuristic approach capable of finding feasible solutions without the need to explicitly define each of these constraints.

4.3. Algorithm

To solve large instances of Problem (3.2), we develop a custom metaheuristic algorithm. Algorithm 1 outlines the overall structure of our solution approach, while Figure 2 illustrates the hierarchical dependencies among the algorithm's operators. At a high level, the algorithm:

- i) Builds a reactive dynamic user optimum (RDUO).
- ii) Builds a solution that greedily routes trips to minimize the system's total travel time.

iii) Chooses the better of i) and ii) to initialize a LNS for further improvement.

These solution-finding modules rely on several intermediate-level operators:

- i) An *insert* operator assigning trips to partial solutions.
- ii) A *local search* that adjusts routes and departure times for inserted trips.
- iii) A *remove* operator that eliminates trips from a solution.

The *insert* and *local search* operators share a common low-level logic for identifying route and departure time combinations. After any insertion or removal, the algorithm evaluates the updated solution. Since evaluation constitutes the most computationally expensive step, we develop an efficient procedure to perform it. As we allow the algorithm to explore intermediate infeasible solutions, the algorithm ranks solutions π using the following cost function:

$$C(\pi) = D(\pi) + \alpha \cdot I(\pi),$$

where $D(\pi)$ is the *total delay* and $I(\pi)$ is the *total infeasibility* associated with π , and α controls the penalty applied to infeasibility. The total delay $D(\pi)$ measures the excess travel time relative to the shortest possible free-flow travel times. It consists of two components: a *detour delay*, the extra time from selecting routes longer in distance than the shortest routes, and a *congestion delay*, the additional time caused by traffic congestion along the chosen routes. The infeasibility term $I(\pi)$ quantifies the total excess travel time of trips arriving later than their latest allowed arrival times.

The remainder of this section is organized as follows. First, we describe the solution-finding modules in Section 4.3.1, followed by the intermediate operators in Section 4.3.2. Finally, we present the lower-level operators in Section 4.3.3.

4.3.1. Solution-finding modules

Reactive dynamic user optimum The RDUO models users departing at their preferred times and independently selecting routes that minimize their travel time based on prevailing traffic con-

Algorithm 1 Framework overview

Input: Set of trips \mathcal{R} , parameters for LNS and routing

- 1: $\pi_{\text{RDUO}} \leftarrow \text{BUILD RDUO}(\mathcal{R})$
 - 2: $\pi_{\text{greedy}} \leftarrow \text{GREEDY ASSIGNMENT}(\mathcal{R})$
 - 3: $\pi \leftarrow \arg \min\{C(\pi_{\text{RDUO}}), C(\pi_{\text{greedy}})\}$
 - 4: $\pi \leftarrow \text{LNS}(\pi)$
 - 5: **return** π
-

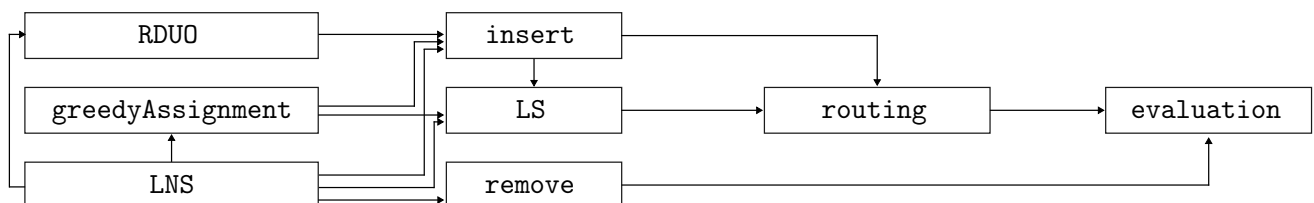


Figure 2: Algorithm operators in hierarchical order. Solution-finding modules (left) generate or improve solutions by invoking intermediate-level operators (center), which, in turn, rely on lower-level logic for routing trips and evaluating the resulting solutions (right).

Algorithm 2 LARGE NEIGHBORHOOD SEARCH

Input: Set of trips \mathcal{R} , π_{greedy} , π_{RDUO} , removal pool size x , destruction percentage y , max cycles z

```

1:  $\pi \leftarrow \arg \min\{C(\pi_{\text{RDUO}}), C(\pi_{\text{greedy}})\}$ 
2: while True do
3:   improved  $\leftarrow$  False
4:   for operator in {COSTLY_TRIPS, UNTOUCHED_TRIPS} do
5:      $\tilde{\pi} \leftarrow \pi$  ▷ Best candidate for this operator
6:      $\mathcal{R}_p \leftarrow \text{SELECTREMOVALPOOL}(\pi, x, \textit{operator})$ 
7:     for  $i$  in  $\{1 \dots z\}$  do
8:        $\mathcal{R}_d \leftarrow \text{RANDOMSAMPLE}(\mathcal{R}_p, y)$ 
9:       for order in SHUFFLE(EARLIEST, LATEST, DELAY) do
10:         $\pi' \leftarrow \text{REMOVE}(\pi, \mathcal{R}_d)$ 
11:         $\pi' \leftarrow \text{INSERT}(\pi', \mathcal{R}_d, \textit{order})$ 
12:        if  $C(\pi') < C(\pi)$  then
13:           $\pi \leftarrow \pi'$ 
14:          improved  $\leftarrow$  True
15:          goto line 6 ▷ Select new removal pool with this operator
16:        else if  $C(\pi') < C(\tilde{\pi})$  then
17:           $\tilde{\pi} \leftarrow \pi'$ 
18:         $\mathcal{R}_c \leftarrow \text{SELECTCHANGEDTRIPS}(\tilde{\pi}, \pi)$ 
19:         $\pi' \leftarrow \text{LOCALSEARCH}(\tilde{\pi}, \mathcal{R}_c)$ 
20:        if  $C(\pi') < C(\pi)$  then
21:           $\pi \leftarrow \pi'$ 
22:          improved  $\leftarrow$  True
23:   if not improved then
24:     break ▷ No improvement in any operator
25: return  $\pi$ 

```

ditions at the time of departure. As users do not account for future congestion, their chosen routes remain fixed once the journey commences. The RDUO computation starts with an empty solution $\pi = (p, s)$, where $p = \emptyset$ and $s = \emptyset$ denote the initial route and departure time assignment sets. The procedure inserts trips sequentially, in order of increasing departure times. For each trip, $s \leftarrow s \cup e^r$ and $p \leftarrow p \cup p_e^r$, where p_e^r minimizes travel time at e^r given previously assigned trips. We provide the pseudocode in Appendix B.

Greedy assignment The greedy assignment sequentially adds trips to an initially empty solution, selecting staggering and routing options to minimize total system travel time. As in the RDUO, the algorithm starts from an empty solution and inserts trips one at a time. This process may yield infeasible solutions, as the greedy insertion of early trips can cause later trips to violate their latest arrival times. To address this, the algorithm prioritizes the insertion of trips with the most restrictive latest arrival times, thereby promoting feasibility while still minimizing total delay. If infeasibilities remain at the end of the insertion procedure, the algorithm invokes a *local search*, which assigns new route and departure time combinations to late-arriving trips as a repair mechanism. We include the corresponding pseudocode in Appendix B.

Large neighborhood search The LNS iteratively improves a solution by progressively selecting destroy and repair operators applied to subsets of trips, thereby gradually exploring better combinations of trip routes and departure times. Algorithm 2 summarizes the steps of the LNS. The

algorithm begins by selecting the lower-cost solution between the RDUO and the greedy assignment as the *incumbent* (1.1). Each iteration begins by selecting the *remove* operator, applying one of the following strategies:

- i) removal of the trips with the highest individual cost;
- ii) removal of the trips scheduled earliest along their shortest-distance route.

These two operators target distinct classes of trips, yet both offer strong potential for improvement: the first removes the most costly trips that contribute significantly to the overall solution cost, while the second focuses on reassigning trips with untapped potential for improved balancing or staggering. After the operator selection, the algorithm builds a removal pool (1.6) consisting of $x\%$ of all trips, along with any infeasible ones. Up to z attempts (1.7), it randomly samples $y\%$ of the pool (1.8) and removes the selected trips from the current solution (1.10). It then uses the *insert* operator to reinsert the removed trips, which explores up to three insertion orders applied in random sequence (1.9–11): If any reinsertion produces a new incumbent solution, the algorithm immediately restarts the destroy-repair cycle by selecting a new removal pool using the last remove operator invoked (1.13–15). If no incumbent updates occur after z cycles, the algorithm invokes the *local search* procedure to improve the quality of the best solution found from this phase (1.18–22). While effective, the local search is computationally expensive, as it operates on full solutions. Therefore, during its first invocation, the algorithm applies the local search to all trips in \mathcal{R} , and restricts it in subsequent calls to trips whose delay or infeasibility has changed since the previous invocation. To support this, the algorithm maintains two vectors storing each trip’s total delay and infeasibility, updated after every *local search* call.

After completing the local search, the algorithm proceeds to the next destroy operator. If at least one incumbent update occurs after evaluating all destroy operators, the algorithm restarts from the first operator (1.22). Otherwise, it terminates (1.24) and returns the best solution found (1.25).

To help the LNS balance feasibility and solution quality, we utilize an adaptive infeasibility weight α , which penalizes constraint violations in the solution cost. Starting with α equal to ten, we divide it by ten if ten consecutive *insert* calls yield feasible solutions, thereby reducing the penalty and encouraging exploration near the boundary of the feasible region. Conversely, if ten consecutive calls result in infeasible solutions, we multiply α by ten to guide the search back toward feasibility. To prevent both excessive penalization and loss of feasibility, we constrain α to the interval $[10^{-2}, 10^3]$.

4.3.2. Intermediate-level operators

Insert The *insert* operator takes as input a partial solution, a set of trips to insert, and a rule specifying the insertion order. Operating on one trip at a time, it tests and evaluates a series of alternative route and departure time combinations (p^r, s_r) , identified using the low-level *routing* logic. It selects the combination yielding the lowest cost and updates the solution by adding the chosen route and departure time, updating $p \leftarrow p \cup p^r$ and $s \leftarrow s \cup s_r$.

Local search The *local search* operator takes as input a solution π and reassigns routes and departure times for a specified subset of its trips. Unlike *insert*, it does not alter the number of trips in the solution. Proceeding in order of earliest permissible departure times e^r , the operator iteratively generates a set of alternative route and departure time combinations (p^r, \underline{s}_r) for each trip using the low-level *routing* logic. It evaluates all combinations, selects the one with the lowest cost, and updates the solution by replacing the trip’s current route and departure time accordingly.

Remove The *remove* operator takes as input a solution and a set of trips to remove. For each trip, the operator deletes the corresponding route and departure time from the solution, updating $p \leftarrow p \setminus p^r$ and $s \leftarrow s \setminus \underline{s}_r$. After removing all specified trips, it evaluates the resulting solution.

4.3.3. Low-level operators

Evaluation Every modification to a solution — whether a trip insertion, removal, departure time shift, or trip rerouting — alters the solution cost, which the algorithm must quantify. Computing $C(\pi)$ requires assessing both the congestion experienced by trips and any late arrivals at their destinations. To this end, the algorithm assigns each solution a *schedule* S , which specifies, for each trip, the set of arc departure times \underline{s}_a^r determined by the selected start times and routes in π . To determine the actual travel time of a trip r on arc a , the algorithm first calculates the flow on the arc, f_a^r , and then applies Equation (3.1). The algorithm calculates f_a^r by counting the number of *conflicts* with other trips r' on the same arc. A conflict occurs when r departs from a after r' has started but before r' has completed its traversal of the arc, including any delays; that is, when $\underline{s}_a^{r'} \leq \underline{s}_a^r < \bar{s}_a^{r'}$. Previous work on staggered routing proposes the CONSTRUCTSCHEDULE procedure to compute a schedule from scratch; we provide its details in Appendix C. While this function still finds application in our algorithm—for instance, after the *remove* operator deletes a subset of trips from the current solution—it becomes inefficient to evaluate a large number of new assignments, as it rebuilds the entire schedule even when the change affects only the trip under consideration. Algorithm 3 outlines our proposed approach for efficiently updating the schedule

Algorithm 3 UPDATESCHEDULE

Input: Schedule S , solution π

- 1: $Q \leftarrow \text{GETCHANGES}(S, \pi)$
- 2: **while** Q is not empty **do**
- 3: $(r, a, \underline{s}_a^r) \leftarrow Q.\text{POP}()$
- 4: $S, r' \leftarrow \text{PROCESSTRIP}(r, a, \underline{s}_a^r)$
- 5: **if** $r' \neq \text{FALSE}$ **then**
- 6: $Q \leftarrow \text{INSERTTRIPS}(r, r', a, \underline{s}_a^r, \underline{s}_a^{r'})$
- 7: **else**
- 8: **while** $r' = \text{FALSE}$ **do**
- 9: $a' \leftarrow \text{GETNEXTARC}(r, a, \pi)$
- 10: $S, r' \leftarrow \text{PROCESSTRIP}(r, a', \underline{s}_a^r)$
- 11: $a \leftarrow a'$
- 12: **if** $r' \neq \text{FALSE}$ **then**
- 13: $Q \leftarrow \text{INSERTTRIPS}(r, r', a, \underline{s}_a^r, \underline{s}_a^{r'})$
- 14: **return** S

during conflict resolution. The core challenge that the algorithm addresses lies in identifying how a modification to a trip's route or departure time propagates through the schedule. In the best case, the change affects only the modified trip; in the worst case, it triggers a cascade of updates that shift the departure times of many other trips. Our method extends the `UPDATESCHEDULE` procedure from previous work on staggered routing by supporting multiple route alternatives and introducing further refinements to improve computational efficiency.

To initiate the search, we begin with an existing schedule that serves as a benchmark for evaluating changes resulting from start time or route adjustments. At the core of the algorithm is a priority queue Q , initially empty. This queue holds tuples that include trip-arc-departure labels $(r, a, \underline{s}_a^r)$. To manage Q , we sort the tuples in ascending order based on their start times \underline{s}_a^r . We fill the queue with all trips potentially impacted by modifications in their scheduled departures (1.1). The approach to populating this queue varies based on the specific operation being executed:

- i) Trip insertion or staggering: We add an initial tuple containing the trip, the first arc of its assigned route, and its scheduled departure time.
- ii) Trip rerouting: We add all trips affected by the change on the previous route to the queue, along with a tuple for the rerouted trip at its earliest entry time on the new route. Specifically, for each arc a along the previous route, we insert $(r', a, \underline{s}_a^{r'})$ for every trip r' that conflicts with the rerouted trip in the original schedule.

We start processing trips in Q (1.3) by checking whether the trip's updated departure time \underline{s}_a^r creates a change in the arc entry times of another trip r' (1.4). In this case, we insert r' into Q . If this insertion disrupts the queue order — specifically, if $\underline{s}_a^{r'} < \underline{s}_a^r$ — we flag the conflict by setting $r' \neq \text{FALSE}$, reinsert \underline{s}_a^r into Q , and restart the evaluation from line 5 to 6. If \underline{s}_a^r does not induce changes ($r' = \text{FALSE}$) in other trips, we recursively propagate the change in trip r 's arc entry times on subsequent arcs until the trip reaches its destination (1.7-13). Our overall update ends once Q is empty and all arc entry times have been correctly adjusted.

To efficiently determine which trips to push to Q and count the resulting conflicts when processing trip r on arc a , we maintain auxiliary sets R_a , which store the labels of all trips currently assigned to arc a , sorted by departure time. We partition this set into:

- i) R_a^I : labels of *inactive* trips, i.e., those not yet enqueued in Q .
- ii) R_a^A : labels of *active* trips, i.e., those already present in Q .

Initially, $R_a^I = R_a$ and $R_a^A = \emptyset$. As the algorithm activates new trips, it removes their labels from each R_a^I for all arcs in their route and adds them to the corresponding R_a^A . We deliberately avoid maintaining R_a^A in sorted order, since active departure times may change multiple times due to propagation effects, making constant re-sorting computationally expensive. We then compute the flow on arc f_a^r as:

$$f_a^r = \underline{f}_a^r + \bar{f}_a^r,$$

where f_a^r and \bar{f}_a^r represent the flows contributed by inactive and active trips, respectively. Since R_a^A is unsorted, we evaluate \bar{f}_a^r by iterating over all active trips:

$$\bar{f}_a^r = \sum_{r' \in R_a^A \setminus \{r\}} \mathbb{I}(s_a^{r'} \leq s_a^r < \bar{s}_a^{r'}).$$

Conversely, we exploit the sorted structure of R_a^I to compute f_a^r through an efficient counting procedure: we locate the latest trip r' in R_a^I with $\underline{s}_a^{r'} < \underline{s}_a^r$ and traverse the set backward from that position, incrementing a counter at each step, until we find a trip with $\bar{s}_a^{r'} \leq \underline{s}_a^r$. When the FIFO property does not hold on an arc, the procedure may yield occasional inaccuracies in delay calculations. We therefore repair the schedule upon completion of each operator by invoking `CONSTRUCTSCHEDULE`. Finally, the algorithm calculates the corresponding delay using the delay function $d(f_a^r)$ defined in Equation (3.1).

The algorithm adds trip r' to Q if an update to r either introduces a new conflict or resolves an existing one between r and r' . To identify such trips efficiently, we leverage the sorted structure of R_a^I . We define four indices in R_a^I , each representing the insertion position of r based on:

- i) its departure time *before* the update (i_{old}).
- ii) its departure time *after* the update (i_{new}).
- iii) its arrival time *before* the update (j_{old}).
- iv) its arrival time *after* the update (j_{new}).

Trips located between i_{old} and i_{new} (departure range) or between j_{old} and j_{new} (arrival range) become active, as their conflict status with r has changed. Trips outside both ranges remain inactive. Those within the intersection of the two ranges also stay inactive, since their conflict status with r is unaffected. Figure 3 illustrates these cases with an example.

Routing This operator identifies new combinations of start times and routes, either to insert a trip with minimal impact on the solution cost (*insert*) or to improve an existing assignment (*local search*). First, it iteratively refines the departure time on the trip’s initial route to maximize the number of resolved conflicts. As an additional refinement step, the method removes portions of the applied departure shifts that do not contribute to reducing the solution cost, thereby promoting parsimonious staggering. Then, it reroutes the trip as early as possible on each alternative route and repeats the iterative start time identification procedure. After evaluating all routes, it selects

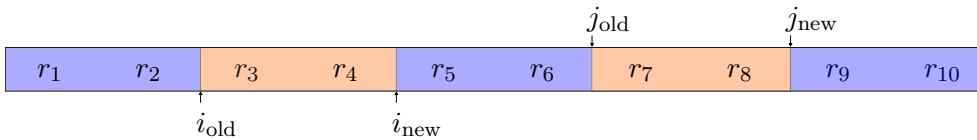


Figure 3: Identification of trips to activate on an arc, given a set of labels sorted by departure time. The indices i_{old} and i_{new} mark the previous and updated departure times of trip r , while j_{old} and j_{new} correspond to its previous and updated arrival times. Trips before (r_1, r_2), after (r_9, r_{10}), or overlapping (r_5, r_6) remain unaffected (highlighted in blue). The algorithm pushes the remaining trips (highlighted in orange) to Q because their conflict status with r changes: either the update resolves a previous conflict (r_3, r_4) or introduces a new one (r_7, r_8).

the route–departure time combination that yields the lowest cost. Figure 4 illustrates this process using a small example. Given a trip r , the algorithm analyzes conflicts along its current route p^r on an arc-by-arc basis, based on its current departure time. On each arc a of the route, the algorithm evaluates whether delaying r can resolve conflicts without introducing new ones. These evaluations are performed independently for each arc and ignore how staggering affects delays on preceding arcs, which may, in turn, influence downstream conflicts. As a result, the conflict-based evaluation serves only as a heuristic proxy for the true impact on overall solution quality.

To detect conflicts efficiently, the algorithm uses the sorted set R_a , which orders trip labels on arc a by their departure times. It locates r in R_a and identifies the immediately preceding trip r' . If $\bar{s}_a^{r'} < \underline{s}_a^r$, no overlap occurs, and the algorithm proceeds to the next arc. Otherwise, it delays r just enough to eliminate the conflict, as long as the new departure time remains within its feasible window:

$$s^r \leftarrow \min \left(s^r + \left(\bar{s}_a^{r'} - \underline{s}_a^r \right), e^r + \bar{\sigma}^r \right).$$

If trips on the arc follow a FIFO discipline, resolving the conflict with r' also eliminates all earlier conflicts on the arc. While this assumption does not always hold, the algorithm adopts it as a computational shortcut. After updating the departure time of r , the algorithm first estimates its new arrival time, incorporating both the applied staggering and any delay reductions due to resolved conflicts with preceding trips. It then scans forward through R_a to detect changes in conflict status with subsequent trips r'' . A new conflict arises if $\bar{s}_a^r > \underline{s}_a^{r''}$, whereas no such conflict existed before the update. Conversely, a conflict is resolved if the reduced delay leads to $\bar{s}_a^r \leq \underline{s}_a^{r''}$. The algorithm aggregates all resolved conflicts as f_a^- , and all newly introduced conflicts as f_a^+ , and computes the net conflict gain as:

$$\Delta f_a = f_a^- - f_a^+.$$

This value heuristically indicates the benefit of setting the trip’s start time to s^r on arc a . After evaluating all arcs, the algorithm selects the departure time candidate with the highest net conflict gain Δf_a . If the adjustment improves the solution, the algorithm accepts it and continues refining the start time on the same route until it finds no additional improvement. Before concluding the analysis of the current route, the method trims any part of the applied departure shift that does not

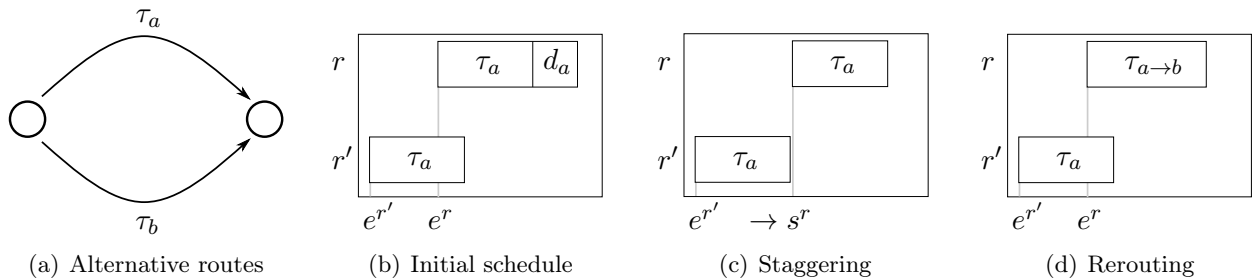


Figure 4: Examples of new start times and route identification on alternative routes a and b , with $\tau_a < \tau_b$.

reduce the solution cost. This refinement brings two main advantages: it unlocks further staggering opportunities for the same trip in later iterations and minimizes overlap with downstream trips on shared arcs. To compute the maximum feasible forward shift for a trip, we examine each arc along its path and determine how much earlier it can depart without introducing new conflicts. For each arc a , we define R'_a as the set of trips $r' \in R_a$ such that $s_a^{r'} < s_a^r$. If $R'_a \neq \emptyset$, we compute the shift to apply to r 's departure time to match it with the latest departure or arrival time among these preceding trips as follows:

$$\Delta s(a) = s_a^r - \max_{r' \in R'_a} \{s_a^{r'}, \bar{s}_a^{r'}\}.$$

We shift the trip's departure time forward by the smallest $\Delta s(a)$ across all arcs, as long as the resulting time respects feasibility constraints. Formally:

$$s^r \leftarrow \max \left(e^r, s^r - \min_{a \in p^r} \Delta s(a) \right).$$

Once the procedure converges on the currently selected route, the algorithm resets r 's departure time to e^r and proceeds to evaluate the next available route. For each alternative route, it applies the same start time selection strategy. After exploring all route options, the algorithm selects the route–departure time combination that yields the lowest overall cost.

To conclude this section, we note that by slightly modifying the logic of the *routing* operator, we can disable either the departure time assignment or the route assignment, resulting in variants that solve only the staggering or balancing problem, respectively. In our case study, we use these modes to isolate and compare the individual contribution of each component to the algorithm's overall performance.

5. Design of experiments

In this section, we present the setup for our case study, including the preparation of the street network, the parameterization of the travel time function, and the trip design. We conclude with a description of the algorithm specifics.

Network We obtain the street network for Manhattan, New York City, from OpenStreetMap (OpenStreetMap 2024). As part of preprocessing, we remove motorway roads, retain only the shortest arc among parallel connections between the same node pair, and consolidate intersections located within a 20-meter radius. Rather than using the entire street network, we extract the southernmost 10% of nodes and their connecting arcs, then retain the largest strongly connected component. The resulting network consists of 302 nodes and 734 arcs. We compute the nominal travel time on each arc by assuming a constant speed of 20 kilometers per hour.

Trip design To model realistic traffic demand, we estimate the number of trips within our study area based on empirical data. During the evening peak on a typical fall weekday, approximately

70000 motorized vehicles — including both base load and taxi demand — enter and leave Manhattan’s Central Business District (NYMTC 2023). Assuming this approximates the total number of trips within Manhattan, and given that our study focuses on a subnetwork covering roughly 10% of the area, we scale this value accordingly and consider 7000 trips per instance to be a reasonable estimate.

We consider 31 instances, one for each day of a month. For each instance, we construct the trip set \mathcal{R} using the 2009 NYC Taxi & Limousine Commission dataset (NYCTL 2009), which provides origin, destination, and departure time information for individual taxi trips. We include all trips with both origin and destination located within the subnetwork over the full 24-hour period of each day, using data from the months of January, March, May, and July (i.e., all 31-day months). To simulate realistic congestion, we compress the departure times into a one-hour window while preserving the original minute and second resolution. This procedure yields instances with an average of approximately 6000 trips, which aligns well with our target scale.

The design of alternative routes is central to the characterization of trip data in our case study. It affects both traffic balancing in our algorithmic solutions and congestion levels observed in the RDUO baseline, as trips in both settings select routes from the same predefined set. We solve the kSPwLO problem with a limited overlap setting the number of alternative paths k to five and the similarity threshold θ to 60%. This choice aligns with the goal of ensuring good network coverage through alternative routes, both to reproduce realistic congestion levels in RDUO and to facilitate traffic balancing, while keeping the number of alternatives small enough to maintain a manageable search space. We discuss this design choice in further detail in Appendix D.

To complete the trip’s characterization, we define each trip’s latest arrival time ℓ^r based on the travel time observed in the RDUO solution, extended by 25% to account for congestion variability. We also set the maximum staggering time $\bar{\sigma}^r$ to 20% of the shortest-route free-flow travel time. We provide a detailed overview of all instances in Appendix E.

Delay function parameterization We characterize the delay function $d(f_a^r)$ as a polynomial expression of the form:

$$d(f_a^r) = \tau_a \cdot \alpha \left[\left(\frac{f_a^r + \beta}{\tau_a} \right)^\gamma - \left(\frac{\beta}{\tau_a} \right)^\gamma \right],$$

where α controls the overall scaling of the delay, β introduces a baseline shift to regulate delays under low congestion, and γ is the polynomial exponent. The subtraction term ensures that the delay function evaluates to zero in the absence of other trips.

To parameterize this function, we used data from the TLC dataset, which includes pickup times, drop-off times, and trip distances. Assuming a constant free-flow speed of 20 km/h, we computed the free-flow travel time and compared it with the trip-recorded durations. In the same network area considered for our experiments, the data indicate a median delay of approximately one and a half minutes during peak hours. Furthermore, commercial mapping services report that travel

between the Financial District and Lower Manhattan experiences a delay of approximately 25% relative to the free-flow travel time during the peak hour.

Given these observations, we set the parameters of the delay function to $\alpha = 0.1$, $\beta = 35$, and $\gamma = 3$. This configuration yields instances with a RDUO characterized by an average total delay representing 12% of the total travel time, and individual trip delays with a median of approximately 0.7 minutes. Although these figures indicate that our instances may underestimate real-world congestion, they effectively serve to demonstrate the core concepts of our algorithm.

Algorithm specifics We configure the LNS algorithm with the following parameters: an initial pool size of $x = 40\%$, a sample size of $y = 10\%$ drawn from this pool, and a maximum of $z = 2$ destroy-repair cycles before invoking the local search for intensification. These values reflect the outcome of a structured parametric analysis, which we report in detail in Appendix F.

6. Results

In this section, we present the results of our numerical experiments. As a first step, we compare the staggering-only variant of our algorithm with the matheuristic proposed in Coppola et al. (2025) to benchmark performance and demonstrate that the new algorithm consistently outperforms it across different levels of flexibility in trip start times.

We then move to the analysis of an idealized scenario in which we assume full control over all vehicles in the system. This setup allows us to establish an upper bound on the performance achievable through centralized routing. Within this framework, we isolate the individual effects of staggering and balancing on fleet and network performance and compare them to the performance of the fully integrated algorithm.

We then examine how to apply staggering and balancing in practice, assess their impact on individual travel and arrival times, and analyze how centralized control reshapes the spatial distribution of congestion. To complement this analysis, we consider more realistic scenarios in which only a portion of the traffic is under centralized control. We explore this from two perspectives: first, a municipality aiming to minimize total system-wide travel time; second, a profit-oriented AMoD service provider focused solely on minimizing the travel time of its own fleet.

We implemented our metaheuristic in C++ and compiled it using GCC version 11.1.0 with `-O3` optimization flags. We ran all experiments on an Intel(R) i9-9900 CPU at 3.1 GHz with 10 GB of RAM. The full implementation and experimental setup are available at https://github.com/tumBAIS/integ_bal_stag.

6.1. Comparison with matheuristic baseline

Figure 5 compares the performance of our staggering-only algorithm, **STAG**, with the matheuristic **MATH** from the literature, using relative delay reduction as the performance metric. We evaluate both methods on a set of 31 instances under two levels of departure-time flexibility: $\bar{\sigma} \downarrow$, where the

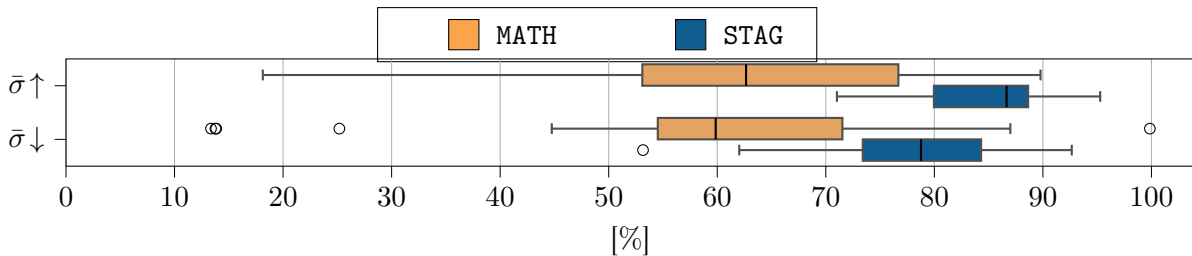


Figure 5: Relative delay reductions achieved by STAG and MATH under reduced ($\bar{\sigma} \downarrow$) and increased ($\bar{\sigma} \uparrow$) levels of flexibility in trip start times.

maximum allowable start time shift $\bar{\sigma}_r$ is set to 10% of the nominal travel time along each trip’s assigned route, and $\bar{\sigma} \uparrow$, where this shift is increased to 20%. For a detailed description of the experimental instances, we refer to Appendix G.

STAG outperforms MATH in terms of median delay reduction by approximately 20 and 25 percentage points under $\bar{\sigma} \downarrow$ and $\bar{\sigma} \uparrow$, respectively. Interestingly, increasing flexibility from $\bar{\sigma} \downarrow$ to $\bar{\sigma} \uparrow$ brings only modest gains for MATH (around 3 percentage points in the median) and coincides with the loss of the sole optimal solution found. This highlights how MATH benefits from tightly bounded departure times, which enable leaner MILP models with fewer big-M constraints. However, as flexibility grows, these structural advantages vanish: the search space becomes more symmetric, relaxations weaken, and performance declines. In contrast, STAG benefits from increased flexibility: its computational complexity and efficiency remain stable even with wider time windows, allowing it to improve median delay reduction by around ten percentage points and enhance robustness through stronger worst-case performance and reduced variance.

Result 1. *Across different levels of flexibility in trip start times, STAG consistently outperforms MATH, delivering higher delay reductions with reduced variance.*

Notably, the instances considered in this comparison already push MATH to its computational limits, since tracking pairwise trip interactions requires an exponential number of constraints, which rapidly increase memory usage. In contrast, STAG circumvents this exponential growth entirely, making it well-suited for large-scale applications. The combination of superior performance and scalability makes STAG the natural choice for solving the staggering-only variant of the problem in the remainder of this study, where the number of pairwise trip interactions is significantly higher than in the present benchmark.

6.2. Algorithmic performance

Figure 6 illustrates the performance of three variants of our algorithm on the instances described in Section 5: BAL, which applies only balancing operations; STAG, which only staggers trip departures; and INTEG, which combines both strategies. The figure reports total and congestion-induced delay reductions relative to RDUO under full traffic control, expressed in both percentage and absolute terms, along with the absolute detour delay introduced by balancing. All experiments terminated within a four-hour time limit.

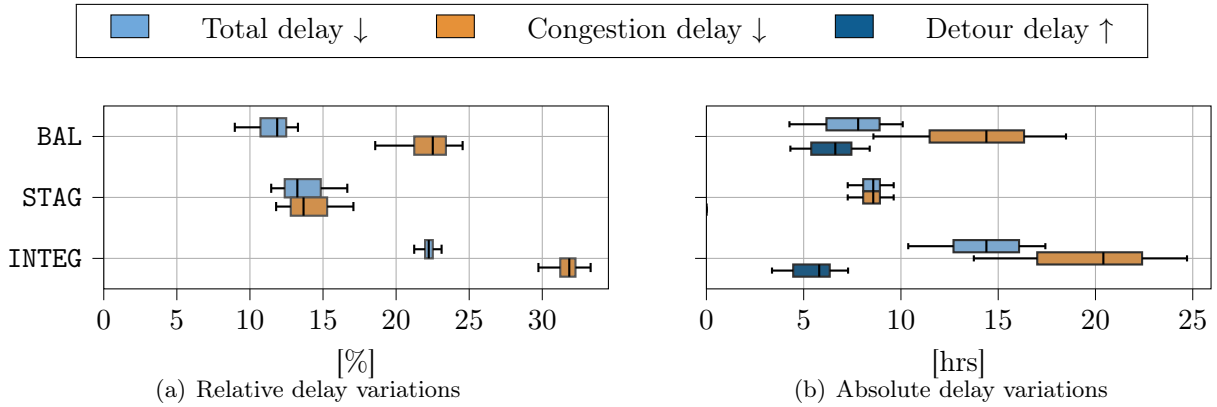


Figure 6: Figure 6(a) shows the relative reductions in total and congestion delay compared to RDU0 under full traffic control. Figure 6(b) shows the corresponding absolute values, including detour delay increases induced by balancing.

Total delay reductions. When isolating individual mechanisms, we observe that balancing alone (BAL) yields a median delay reduction of 12% (approximately 8 hours). This result suggests that self-interested users, unaware of future congestion, often select suboptimal routes, while the balancing operator distributes traffic more efficiently across available paths. Staggering alone (STAG) achieves a comparable median delay reduction of 13% (approximately 9 hours), demonstrating that our greedy staggering strategy, which adjusts departure times to resolve arc-level conflicts without accounting for upstream congestion effects, serves as an effective heuristic proxy for identifying promising trip start times.

The fully integrated algorithm (INTEG) consistently delivers strong performance across all real-world instances, achieving total delay reductions consistently around 23%. In absolute terms, this corresponds to 10 to 17 hours of reduced travel time. Crucially, the integrated approach appears to combine the benefits of both rerouting and rescheduling in a near-additive manner, highlighting their complementary roles in mitigating delay.

Result 2. *The integrated algorithm achieves total delay reductions of 23%, translating into up to 17 hours of saved travel time across the entire system.*

Trade-offs between congestion and detour. From the operator’s perspective, total delay reduction translates directly into shorter travel times and economic savings. Yet, it is equally important to assess network efficiency. Specifically, we assess the reduction in congestion delay, potentially at the cost of increased detour delay.

In STAG, all delay reduction corresponds to congestion relief, since routes remain fixed. Interestingly, balancing alone well mitigates congestion: BAL removes over 23% of congestion-induced delay in median, which translates to approximately 15 hours. However, this improvement comes with additional detour delay — about six hours on average. Remarkably, the integrated approach delivers an even more favorable trade-off. By leveraging staggering to reduce congestion without modifying

routes, INTEG removes more congestion delay compared to balancing alone (up to 25 hours) while inducing less additional detour delays.

Result 3. *The integrated algorithm removes more congestion delay (up to 25 hours) than balancing alone (up to 18 hours), while introducing less detour delays (under 6 hours).*

6.3. Structural analysis

In this section, we analyze the structural characteristics of the solutions generated by different control strategies. Figure 7 presents: (a) the route assignment distribution for the baseline RDUO and for the rebalancing variants BAL and INTEG, (b) the frequency of staggering in STAG and INTEG, (c) travel time differences relative to the baseline, and (d) differences in arrival times.

We first observe that the RDUO configuration tends to overload the shortest available routes. In contrast, both BAL and INTEG redistribute a portion of the demand to longer distance alternatives to mitigate congestion. Expectedly, INTEG assigns a slightly larger fraction of trips to the shortest route than BAL: by also applying staggering, INTEG reduces reliance on detouring to achieve higher performance gains. Regarding staggering behavior, both INTEG and STAG most frequently apply small shifts, as shown by the higher concentration of trips in the zero to twenty-second departure shift bin. Generally, INTEG applies staggering to a larger share of trips and with greater intensity than STAG, highlighting how the additional flexibility offered by route rebalancing unlocks further staggering opportunities. The resulting staggering distribution exhibits a clear decay: most adjustments fall within the first 40 seconds, with diminishing frequency thereafter.

The distribution of travel time differences reveals that achieving system-wide efficiency requires some trips to incur longer travel times. These increases are typically modest, mostly within 15

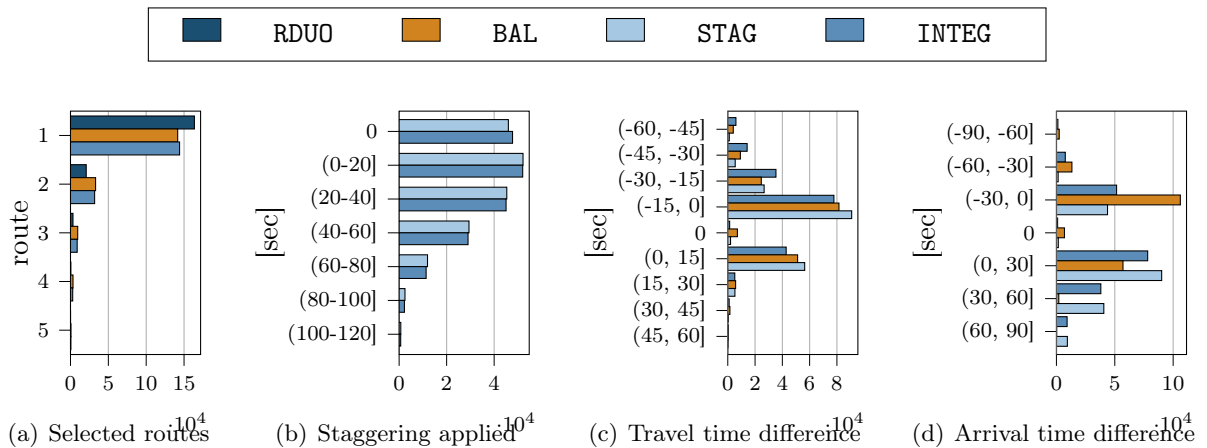


Figure 7: Frequency plots comparing the structure of the baseline and optimized solutions: (a) route assignments, with route IDs sorted from shortest to longest distance; (b) staggering operations applied, where zero indicates no staggering; (c) travel time differences, where negative values indicate shorter travel times in the solution relative to the baseline, and positive values indicate increases; and (d) arrival time differences, where negative values indicate earlier arrivals and positive values indicate delays relative to the baseline.

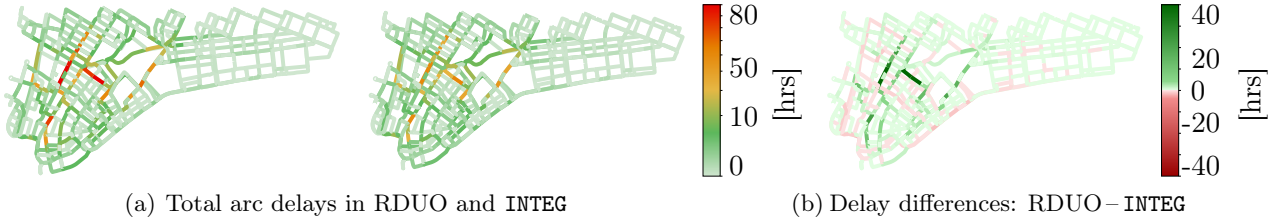


Figure 8: Spatial distribution of arc-level delays over 31-day instances in RDUO and INTEG (a), and their delay differences (b).

seconds, and only a small fraction exceeds 30 seconds. This trade-off is counterbalanced by a greater number of trips benefiting from travel time reductions, with improvements reaching up to 60 seconds. Finally, arrival time differences are distributed almost symmetrically around zero, with only a small fraction of trips arriving at exactly the same time as in the RDUO configuration. In the BAL variant, the distribution is skewed toward earlier arrivals, whereas configurations involving staggering exhibit a slight skew toward positive differences, consistent with their design to delay trips strategically.

Result 4. *Centralized coordination yields solutions that are structurally distinct from RDUO: (i) it alleviates congestion by rebalancing demand away from the shortest routes, (ii) it integrates balancing and staggering to identify larger pools of promising departure times, and (iii) it enhances overall efficiency by allowing slight travel time increases for some trips, while maintaining tight control over arrival times.*

To complement the structural analysis and illustrate how our algorithm reshapes congestion patterns, Figure 8 compares cumulative arc-level delays across all 31-day instances between the RDUO and INTEG solutions. In the RDUO configuration, congestion remains concentrated in the central region of the network. By contrast, the INTEG solution achieves a more balanced traffic distribution, effectively alleviating these bottlenecks, particularly in areas where alternative routes support rerouting. Importantly, this improvement does not cause delay displacement or introduce new congestion hotspots. As illustrated in the differential map, central arcs benefit from substantial delay reductions of up to 40 hours, while newly utilized arcs see only minor increases, typically below 5 hours.

Result 5. *Our algorithm alleviates major bottlenecks, reducing delays by up to 40 hours, without shifting congestion elsewhere. Delay increases on newly utilized arcs remain minimal, generally under 5 hours, effectively preventing the emergence of new congestion points.*

6.4. Flow control analysis

This section analyzes how total delay evolves as the fraction of controlled traffic φ increases. In each instance, trips are randomly designated as AMoD trips with probability φ . Baseload trips follow fixed behavior, consistent with the RDUO solution; we leave the study of responsive baseload

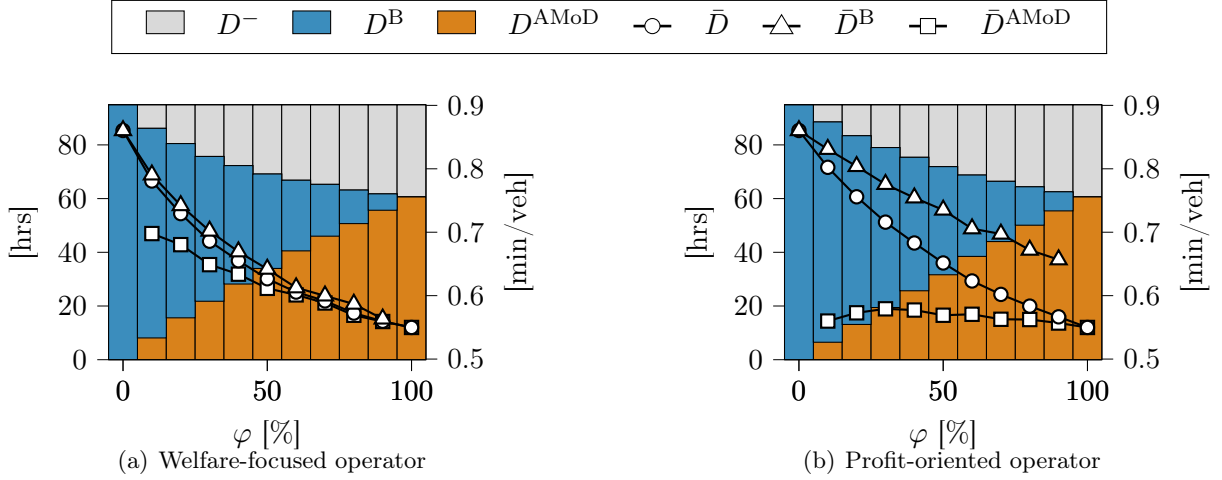


Figure 9: Impact of the controlled traffic fraction φ on total and average delay metrics. Figure 9(a) presents results for a welfare-focused operator aiming to minimize total system travel time. Figure 9(b) shows results for a profit-oriented operator focused on minimizing the travel time of its own fleet. Metrics include total delay removed D^- , baseload traffic delay D^B , fleet delay D^{AMoD} , and average delays for all trips \bar{D} , baseload trips \bar{D}^B , and fleet trips \bar{D}^{AMoD} .

dynamics to AMoD behavior to future work. We consider two control paradigms. In the first, a welfare-oriented authority aims to minimize total system delay by optimizing the travel times of all trips. In the second, a self-interested operator controls only a fleet of AMoD vehicles and minimizes the delay experienced by its own fleet, without accounting for delays among baseload trips.

Figure 9 presents results for a representative instance (day 21), illustrating how system-wide delay evolves as φ increases. In the welfare-oriented case, we observe diminishing returns, with the most substantial marginal delay reductions occurring when fewer than 50% of trips are under control. In contrast, the profit-driven scenario exhibits a more linear trend, as improvements are concentrated on the operator’s own fleet.

In the welfare-driven scenario, average delays for AMoD and baseload trips remain similar, especially for $\varphi > 30\%$. In contrast, the profit-driven controller maintains minimal delay for its fleet, while baseload traffic delays remain relatively high. Despite their differing objectives, both strategies lead to clear reductions in total and average delays for both trip classes, suggesting that even partial control yields substantial system-wide benefits.

Result 6. *Controlling only a fraction of the traffic with staggered and balanced routing yields a win-win outcome: AMoD fleets achieve lower delays, while baseload traffic also benefits from improved flow. These system-wide gains arise regardless of whether the operator optimizes for overall welfare or fleet-specific efficiency.*

7. Conclusion

In this work, we introduced a novel framework for integrating staggered and balanced routing into AMoD system operations. Our approach minimizes fleet travel times while enhancing overall

network efficiency by strategically assigning trips to optimized routes and departure time patterns. We described the problem through a mathematical formulation of the problem and showed that, under mild assumptions, our congestion model provides an unbiased approximation of a discretized Vickrey bottleneck model.

To solve large-scale instances of the problem, we developed a custom metaheuristic based on a LNS framework. In a case study using real-world data from taxi trips in the Manhattan street network, we addressed a realistic volume of peak-hour demand approximating real-world traffic congestion levels. To generate route alternatives, we employed a k -shortest path algorithm with overlap constraints, enabling a diverse yet efficient set of routing options while maintaining computational tractability. Our results show that, under full control, our method can reduce total delays by up to 25% compared to selfish routing. When focusing on network congestion, improvements reach up to 35%. These gains result from redistributing trips onto slightly longer routes and applying modest staggering to departure times. While a small number of trips experience modest travel time increases, the broader gains across the network outweigh these losses. Spatially, the improvements result from congestion relief at bottlenecks, without generating new hotspots elsewhere in the network.

We also examined how the system responds to varying fractions of controlled traffic under two paradigms: a welfare-oriented authority optimizing total system travel time, and a profit-driven AMoD operator focused solely on fleet performance. In both scenarios, staggered and balanced routing consistently improve outcomes for both AMoD and exogenous trips across all control levels.

This research opens several avenues for future work. First, replacing the assumption of pre-computed routes with methods that compute globally optimal ones could unlock further improvements in balancing operations. Second, advancing departure time selection policies may further enhance overall system performance. Third, evaluating the framework under higher congestion levels would provide a more realistic assessment of algorithm performance in real-world conditions. Additionally, incorporating scenarios with incomplete demand information would improve realism and allow benchmarking the cost of limited information. Finally, future work should explore how baseload traffic dynamically adapts to the behavior of AMoD services.

References

- Abraham, I., Delling, D., Goldberg, A. V., & Werneck, R. F. (2013). Alternative routes in road networks. *Journal of Experimental Algorithmics (JEA)*, 18, 1–1.
- Adacher, L., & Tiriolo, M. (2018). A macroscopic model with the advantages of microscopic model: A review of cell transmission model’s extensions for urban traffic networks. *Simulation Modelling Practice and Theory*, 86, 102–119.
- Aghamohammadi, R., & Laval, J. A. (2020). Dynamic traffic assignment using the macroscopic fundamental diagram: A review of vehicular and pedestrian flow models. *Transportation Research Part B: Methodological*, 137, 99–118.
- Alonso-Mora, J., Wallar, A., & Rus, D. (2017). Predictive routing for autonomous mobility-on-demand systems with ride-sharing. In *International Conference on Intelligent Robots and Systems (IROS)*. IEEE.
- Arnott, R., de Palma, A., & Lindsey, R. (1990). Departure time and route choice for the morning commute. *Transportation Research Part B: Methodological*, 24, 209–228.
- Bahrami, S., & Roorda, M. J. (2020). Optimal traffic management policies for mixed human and automated traffic flows. *Transportation Research Part A: Policy and Practice*, 135, 130–143.

- Bang, H., & Malikopoulos, A. A. (2022). Congestion-aware routing, rebalancing, and charging scheduling for electric autonomous mobility-on-demand system. In *2022 American Control Conference (ACC)* (pp. 3152–3157).
- Battifarano, M., & Qian, S. (2023). The impact of optimized fleets in transportation networks. *Transportation Science*, *57*, 1047–1068.
- Carey, M., & Watling, D. (2012). Dynamic traffic assignment approximating the kinematic wave model: System optimum, marginal costs, externalities and tolls. *Transportation Research Part B: Methodological*, *46*, 634–648.
- Chondrogiannis, T., Bouros, P., Gamper, J., Leser, U., & Blumenthal, D. B. (2020). Finding k-shortest paths with limited overlap. *The VLDB Journal*, *29*, 1023–1047.
- Coppola, A., Hiermann, G., Paccagnan, D., & Schiffer, M. (2025). Staggered routing in autonomous mobility-on-demand systems. *European Journal of Operational Research*, . In Press.
- Diao, M., Kong, H., & Zhao, J. (2021). Impacts of transportation network companies on urban mobility. *Nature Sustainability*, *4*, 494–500.
- Enders, T., Harrison, J., Pavone, M., & Schiffer, M. (2023). Hybrid multi-agent deep reinforcement learning for autonomous mobility on demand systems. In *Learning for Dynamics and Control Conference* (pp. 1284–1296). PMLR.
- Estandia, A., Schiffer, M., Rossi, F., Luke, J., Kara, E. C., Rajagopal, R., & Pavone, M. (2021). On the interaction between autonomous mobility on demand systems and power distribution networks—an optimal power flow approach. *IEEE Transactions on Control of Network Systems*, *8*, 1163–1176.
- Friesz, T. L., Kim, T., Kwon, C., & Rigdon, M. A. (2011). Approximate network loading and dual-time-scale dynamic user equilibrium. *Transportation Research Part B: Methodological*, *45*, 176–207.
- Gammelli, D., Yang, K., Harrison, J., Rodrigues, F., Pereira, F. C., & Pavone, M. (2021). Graph neural network reinforcement learning for autonomous mobility-on-demand systems. In *2021 60th IEEE Conference on Decision and Control (CDC)* (pp. 2996–3003). IEEE.
- Geisberger, R., Sanders, P., Schultes, D., & Delling, D. (2008). Contraction hierarchies: Faster and simpler hierarchical routing in road networks. In C. C. McGeoch (Ed.), *Experimental Algorithms* (pp. 319–333). Springer Berlin Heidelberg.
- Han, K., Friesz, T. L., & Yao, T. (2013). Existence of simultaneous route and departure choice dynamic user equilibrium. *Transportation Research Part B: Methodological*, *53*, 17–30.
- Hendrickson, C., & Kocur, G. (1981). Schedule delay and departure time decisions in a deterministic model. *Transportation science*, *15*, 62–77.
- Hu, T.-Y., & Mahmassani, H. S. (1997). Day-to-day evolution of network flows under real-time information and reactive signal control. *Transportation Research Part C: Emerging Technologies*, *5*, 51–69.
- Huang, H.-J., & Lam, W. H. (2002). Modeling and solving the dynamic user equilibrium route and departure time choice problem in network with queues. *Transportation Research Part B: Methodological*, *36*, 253–273.
- Iglesias, R., Rossi, F., Wang, K., Hallac, D., Leskovec, J., & Pavone, M. (2018). Data-driven model predictive control of autonomous mobility-on-demand systems. In *2018 IEEE International Conference on Robotics and Automation (ICRA)* (pp. 1—7). IEEE Press.
- Jalota, D., Paccagnan, D., Schiffer, M., & Pavone, M. (2023). Online routing over parallel networks: Deterministic limits and data-driven enhancements. *INFORMS Journal on Computing*, *35*, 560–577.
- Jauffred, F. J., & Bernstein, D. (1996). An alternative formulation of the simultaneous route and departure-time choice equilibrium problem. *Transportation Research Part C: Emerging Technologies*, *4*, 339–357.
- Jiao, Y., Tang, X., Qin, Z. T., Li, S., Zhang, F., Zhu, H., & Ye, J. (2021). Real-world ride-hailing vehicle repositioning using deep reinforcement learning. *Transportation Research Part C: Emerging Technologies*, *130*, 103289.
- Jungel, K., Parmentier, A., Schiffer, M., & Vidal, T. (2023). Learning-based online optimization for autonomous mobility-on-demand fleet control. *arXiv:2302.03963 [math.OG]*, . doi:10.48550/arXiv.2302.03963.
- Kondor, D., Bojic, I., Resta, G., Duarte, F., Santi, P., & Ratti, C. (2022). The cost of non-coordination in urban on-demand mobility. *Scientific reports*, *12*, 4669.
- Levin, M. W. (2017). Congestion-aware system optimal route choice for shared autonomous vehicles. *Transportation Research Part C: Emerging Technologies*, *82*, 229–247.
- Li, M., Qin, Z., Jiao, Y., Yang, Y., Wang, J., Wang, C., Wu, G., & Ye, J. (2019). Efficient ridesharing order dispatching with mean field multi-agent reinforcement learning. In *The World Wide Web Conference WWW '19* (pp. 983—994). New York, NY, USA: Association for Computing Machinery.
- Li, Z.-C., Huang, H.-J., & Yang, H. (2020). Fifty years of the bottleneck model: A bibliometric review and future research directions. *Transportation research part B: methodological*, *139*, 311–342.

- Liang, E., Wen, K., Lam, W. H., Sumalee, A., & Zhong, R. (2021). An integrated reinforcement learning and centralized programming approach for online taxi dispatching. *IEEE Transactions on Neural Networks and Learning Systems*, *33*, 4742–4756.
- Lindsey, C. R., Van den Berg, V. A., & Verhoef, E. T. (2012). Step tolling with bottleneck queuing congestion. *Journal of Urban Economics*, *72*, 46–59.
- Liu, Y., & Nie, Y. M. (2011). Morning commute problem considering route choice, user heterogeneity and alternative system optima. *Transportation Research Part B: Methodological*, *45*, 619–642.
- Liu, Y., & Samaranayake, S. (2022). Proactive rebalancing and speed-up techniques for on-demand high capacity ridesourcing services. *IEEE Transactions on Intelligent Transportation Systems*, *23*, 819–826.
- Lo, H. K., & Szeto, W. (2002). A cell-based variational inequality formulation of the dynamic user optimal assignment problem. *Transportation Research Part B: Methodological*, *36*, 421–443.
- Long, J., Huang, H.-J., Gao, Z., & Szeto, W. Y. (2013). An intersection-movement-based dynamic user optimal route choice problem. *Operations Research*, *61*, 1134–1147.
- Long, J., Wang, C., & Szeto, W. (2018). Dynamic system optimum simultaneous route and departure time choice problems: Intersection-movement-based formulations and comparisons. *Transportation Research Part B: Methodological*, *115*, 166–206.
- Makridis, C., Menelaou, C., Timotheou, S., & Panayiotou, C. G. (2024). A real-time demand management and route-guidance system for eliminating congestion. *IEEE Intelligent Transportation Systems Magazine*, .
- Menelaou, C., Timotheou, S., Kolios, P., & Panayiotou, C. G. (2021). Joint route guidance and demand management for real-time control of multi-regional traffic networks. *IEEE Transactions on Intelligent Transportation Systems*, *23*, 8302–8315.
- Mounce, R., & Carey, M. (2011). Route swapping in dynamic traffic networks. *Transportation Research Part B: Methodological*, *45*, 102–111.
- Nie, Y. (2010). Solving the dynamic user optimal assignment problem considering queue spillback. *Networks and Spatial Economics*, *10*, 49–71.
- NYCTLC (2009). TLC Trip Record Data. URL: <https://tinyurl.com/tlc-trip-data>.
- NYMTC (2023). Hub bound travel data 2023. URL: <https://tinyurl.com/3bdsvhsd> New York Metropolitan Transportation Council.
- Oh, S., Seshadri, R., Azevedo, C. L., Kumar, N., Basak, K., & Ben-Akiva, M. (2020). Assessing the impacts of automated mobility-on-demand through agent-based simulation: A study of singapore. *Transportation Research Part A: Policy and Practice*, *138*, 367–388.
- OpenStreetMap (2024). URL: <https://www.openstreetmap.org>.
- Otsubo, H., & Rapoport, A. (2008). Vickrey’s model of traffic congestion discretized. *Transportation Research Part B: Methodological*, *42*, 873–889.
- Pavone, M. (2015). Autonomous mobility-on-demand systems for future urban mobility. In *Autonomes Fahren: Technische, rechtliche und gesellschaftliche Aspekte* (pp. 399–416). Berlin, Heidelberg: Springer Berlin Heidelberg.
- Ran, B., Hall, R. W., & Boyce, D. E. (1996). A link-based variational inequality model for dynamic departure time/route choice. *Transportation Research Part B: Methodological*, *30*, 31–46.
- Rossi, F., Iglesias, R., Alizadeh, M., & Pavone, M. (2020). On the interaction between autonomous mobility-on-demand systems and the power network: Models and coordination algorithms. *IEEE Transactions on Control of Network Systems*, *7*, 384–397.
- Rossi, F., Zhang, R., Hindy, Y., & Pavone, M. (2018). Routing autonomous vehicles in congested transportation networks: structural properties and coordination algorithms. *Autonomous Robots*, *42*, 1427–1442.
- Sadeghi Eshkevari, S., Tang, X., Qin, Z., Mei, J., Zhang, C., Meng, Q., & Xu, J. (2022). Reinforcement learning in the wild: Scalable RL dispatching algorithm deployed in ridehailing marketplace. In *Proceedings of the 28th ACM SIGKDD Conference on Knowledge Discovery and Data Mining KDD ’22* (pp. 3838—3848). New York, NY, USA: Association for Computing Machinery.
- Salazar, M., Lanzetti, N., Rossi, F., Schiffer, M., & Pavone, M. (2019). Intermodal autonomous mobility-on-demand. *IEEE Transactions on Intelligent Transportation Systems*, *21*, 3946–3960.
- Skordilis, E., Hou, Y., Tripp, C., Moniot, M., Graf, P., & Biagioni, D. (2021). A modular and transferable reinforcement learning framework for the fleet rebalancing problem. *IEEE Transactions on Intelligent Transportation Systems*, *23*, 11903–11916.
- Statista (2024). Ride-hailing - United States. URL: <https://tinyurl.com/ride-hailing-us>.

- Tang, X., Qin, Z. T., Zhang, F., Wang, Z., Xu, Z., Ma, Y., Zhu, H., & Ye, J. (2019). A deep value-network based approach for multi-driver order dispatching. In *Proceedings of the 25th ACM SIGKDD International Conference on Knowledge Discovery & Data Mining KDD '19* (pp. 1780–1790). New York, NY, USA: Association for Computing Machinery.
- Thomopoulos, N. T. (2012). *Fundamentals of queuing systems: statistical methods for analyzing queuing models*. Springer Science & Business Media.
- Tsao, M., Iglesias, R., & Pavone, M. (2018). Stochastic model predictive control for autonomous mobility on demand. In *2018 21st International Conference on Intelligent Transportation Systems (ITSC)* (pp. 3941–3948).
- Tsao, M., Milojevic, D., Ruch, C., Salazar, M., Frazzoli, E., & Pavone, M. (2019). Model predictive control of ride-sharing autonomous mobility-on-demand systems. In *2019 International Conference on Robotics and Automation (ICRA)* (pp. 6665–6671).
- Ukkusuri, S. V., Han, L., & Doan, K. (2012). Dynamic user equilibrium with a path based cell transmission model for general traffic networks. *Transportation Research Part B: Methodological*, 46, 1657–1684.
- Vickrey, W. S. (1969). Congestion theory and transport investment. *The American economic review*, 59, 251–260.
- Xu, Z., Li, Z., Guan, Q., Zhang, D., Li, Q., Nan, J., Liu, C., Bian, W., & Ye, J. (2018). Large-scale order dispatch in on-demand ride-hailing platforms: A learning and planning approach. In *Proceedings of the 24th ACM SIGKDD International Conference on Knowledge Discovery & Data Mining KDD '18* (pp. 905–913). New York, NY, USA: Association for Computing Machinery.
- Yang, H., & Meng, Q. (1998). Departure time, route choice and congestion toll in a queuing network with elastic demand. *Transportation Research Part B: Methodological*, 32, 247–260.
- Zanardi, A., Sessa, P. G., Käslin, N., Bolognani, S., Censi, A., & Frazzoli, E. (2023). How bad is selfish driving? bounding the inefficiency of equilibria in urban driving games. *IEEE Robotics and Automation Letters*, 8, 2293–2300.
- Zardini, G., Lanzetti, N., Pavone, M., & Frazzoli, E. (2022). Analysis and control of autonomous mobility-on-demand systems. *Annual Review of Control, Robotics, and Autonomous Systems*, 5, 633–658.
- Zhang, L., Hu, T., Min, Y., Wu, G., Zhang, J., Feng, P., Gong, P., & Ye, J. (2017). A taxi order dispatch model based on combinatorial optimization. In *Proceedings of the 23rd ACM SIGKDD International Conference on Knowledge Discovery and Data Mining KDD '17* (pp. 2151–2159). New York, NY, USA: Association for Computing Machinery.
- Zhou, M., Jin, J., Zhang, W., Qin, Z., Jiao, Y., Wang, C., Wu, G., Yu, Y., & Ye, J. (2019). Multi-agent reinforcement learning for order-dispatching via order-vehicle distribution matching. In *Proceedings of the 28th ACM International Conference on Information and Knowledge Management CIKM '19* (pp. 2645–2653). New York, NY, USA: Association for Computing Machinery.
- Ziliaskopoulos, A. K., & Rao, L. (1999). A simultaneous route and departure time choice equilibrium model on dynamic networks. *International Transactions in Operational Research*, 6, 21–37.
- Ziliaskopoulos, A. K., Waller, S. T., Li, Y., & Byram, M. (2004). Large-scale dynamic traffic assignment: Implementation issues and computational analysis. *Journal of Transportation Engineering*, 130, 585–593.

Appendix A Theorem 1 proof

Proof Consider the travel time function defined in equation (3.3). Taking expectations, we have:

$$\mathbb{E}[T(t)] = \tau_a + (\phi \cdot \tau_a)\mathbb{E}[f(t)].$$

To find the expected number of trips $\mathbb{E}[f(t)]$ in the system, we apply Little's Law, which relates the expected number of trips in a stable system to the arrival rate and the expected time a trip spends in the system:

$$\mathbb{E}[f(t)] = \lambda\mathbb{E}[T(t)].$$

Substituting the expression for $\mathbb{E}[T(t)]$ into $\mathbb{E}[f(t)]$, we have:

$$\begin{aligned} \mathbb{E}[f(t)] &= \rho + (\phi \cdot \rho)\mathbb{E}[f(t)] \\ \implies \mathbb{E}[f(t)] - (\phi \cdot \rho)\mathbb{E}[f(t)] &= \rho \\ \implies \mathbb{E}[f(t)] &= \rho \cdot (1 - \phi \cdot \rho)^{-1}. \end{aligned}$$

The expected number of trips $\mathbb{E}[f(t)]$ is finite when the condition $\phi \cdot \rho < 1$ holds. Since $\phi \in (0, 1]$ and $\rho \in (0, 1)$, this inequality is always satisfied, ensuring system stability for any valid choice of ϕ . Substituting $\mathbb{E}[f(t)]$ back into the expression for $\mathbb{E}[T(t)]$:

$$\mathbb{E}[T(t)] = \tau_a + (\phi \cdot \tau_a)\mathbb{E}[f(t)] = \tau_a + (\phi \cdot \tau_a \cdot \rho)(1 - \phi \cdot \rho)^{-1}.$$

To match the expected travel time with that of Vickrey's model in Equation (3.5), we set:

$$\begin{aligned} \tau_a + (\phi \cdot \tau_a \cdot \rho) \cdot (1 - \phi \cdot \rho)^{-1} &= \tau_a + (\tau_a \cdot \rho) \cdot (2(1 - \rho))^{-1} \\ \implies (\phi \cdot \tau_a \cdot \rho) \cdot (1 - \phi \cdot \rho)^{-1} &= (\tau_a \cdot \rho) \cdot (2(1 - \rho))^{-1} \\ \implies \phi \cdot (1 - \phi \cdot \rho)^{-1} &= 2(1 - \rho)^{-1} \\ \implies 2\phi \cdot (1 - \rho) &= 1 - \phi \cdot \rho. \end{aligned}$$

Rearranging the expression to solve for ϕ gives:

$$\phi = (2 - \rho)^{-1}.$$

Since $0 < \rho \leq 1$, it follows that $\phi \in (0, 1]$. This demonstrates that, for this choice of ϕ , the expected travel time $\mathbb{E}[T(t)]$ matches the expected travel time in Vickrey's model. \square

Appendix B Solution-finding modules pseudocode

We provide pseudocode for the two baseline assignment procedures used to generate initial solutions: the reactive dynamic user optimum (BUILDRDUO) in Algorithm 4, and the greedy assignment heuristic in Algorithm 5.

Algorithm 4 BUILDRDUO**Input:** Set of trips \mathcal{R}

-
- ```

1: $\pi \leftarrow (\emptyset, \emptyset)$ ▷ Initialize empty solution.
2: $\pi \leftarrow \text{INSERTATEARLIESTTIMES}(\pi, \mathcal{R}, \text{EARLIEST})$ ▷ Insert trips by increasing e^r .
3: return π

```
- 

**Algorithm 5** GREEDYASSIGNMENT**Input:** Set of trips  $\mathcal{R}$ 

- 
- ```

1:  $\pi \leftarrow (\emptyset, \emptyset)$  ▷ Initialize empty solution.
2:  $\pi \leftarrow \text{INSERT}(\pi, \mathcal{R}, \text{DEADLINE})$  ▷ Insert trips with tightest  $\ell^r$  first.
3:  $\mathcal{R}^I \leftarrow \text{GETINFEASIBLETRIPS}(\pi)$ 
4: if  $\mathcal{R}^I \neq \emptyset$  then
5:    $\pi \leftarrow \text{LOCALSEARCH}(\pi, \mathcal{R}^I)$ 
6: return  $\pi$ 

```
-

Appendix C Description of constructSchedule

Algorithm 6 details the procedure to construct the schedule S associated with π . We start by sorting the trip start times s^r into a priority queue Q and initialize an empty set \mathcal{T}_a for each arc a to track when each trip completes the traversal of a . Then, we construct an initial solution iteratively:

- i) We start by extracting the departure time \underline{s}_a^r with the highest priority from Q .
- ii) We then set $f_a^r = |\{\bar{s}_a^{r'} \in \mathcal{T}_a \mid \underline{s}_a^r < \bar{s}_a^{r'}\}|$, that is the number of trips that have not completed their traversal of arc a by time \underline{s}_a^r , and compute $d_a^r = d(f_a^r)$.
- iii) Finally, we add the time in which the arc traversal is completed, which is $\underline{s}_a^r + d_a^r + \tau_a$, to \mathcal{T}_a by setting $\mathcal{T}_a = \mathcal{T}_a \cup (\underline{s}_a^r + d_a^r + \tau_a)$. If a is not the last arc of route p^r , we insert $\underline{s}_a^r + d_a^r + \tau_a$ into Q .

We repeat these steps until Q is empty.

Appendix D Alternative route design

In this section, we explain the rationale for selecting alternative routes for trips by solving a kSP-wLO problem. The aim is to find k routes connecting an origin-destination pair, each as short as possible, while ensuring that any two have at most θ % of shared path length. An important consideration is that the route selection influences both our baseline RDUO solution and our proposed algorithmic solutions since both draw routes from the same candidate set. Thus, choosing appropriate parameters k and θ is crucial. Figure 10 illustrates the total delays in the RDUO across the 31 instances considered for various combinations of k and θ . Evidently, higher values of k in conjunction with larger θ values provide users with greater flexibility in their route choices, resulting in the smallest median total delay (approximately 78 hours) observed for configurations where $\theta = 0.9$ and $k \geq 7$. However, since our algorithm aims to evenly distribute traffic across alternative network segments to enhance overall efficiency, diversity in route selection becomes highly beneficial. In particular, the scenario with $\theta = 0.6$ and $k = 5$ leads to an increase in median delay of approximately five hours compared to the optimal flexible scenario ($\theta = 0.9$ and $k \geq 7$). We consider this trade-off acceptable given the clear advantage of promoting more diverse route choices and consequently improved network balance.

Algorithm 6 CONSTRUCTSCHEDULE

Input: Solution π

- 1: $Q \leftarrow \text{INITIALIZEPRIORITYQUEUE}(\pi)$
- 2: $S \leftarrow \text{INITIALIZESCHEDULE}(\pi)$
- 3: **while** Q is not empty **do**
- 4: $(r, a) \leftarrow Q.\text{POP}()$
- 5: $f_a^r \leftarrow \text{COMPUTEFLOWONARC}(\underline{s}_a^r)$
- 6: $d_a^r \leftarrow \text{COMPUTEDELAY}(f_a^r)$
- 7: $a' \leftarrow \text{GETNEXTARC}(r, a, \pi)$
- 8: $\underline{s}_{a'}^r \leftarrow \underline{s}_a^r + \tau_a + d_a^r$
- 9: $S \leftarrow \text{ADDDPARTURE}(\underline{s}_{a'}^r)$
- 10: **if** $a' \neq \bar{a}_r$ **then**
- 11: $Q \leftarrow \text{PUSHTRIP}(r, a')$
- 12: **return** S

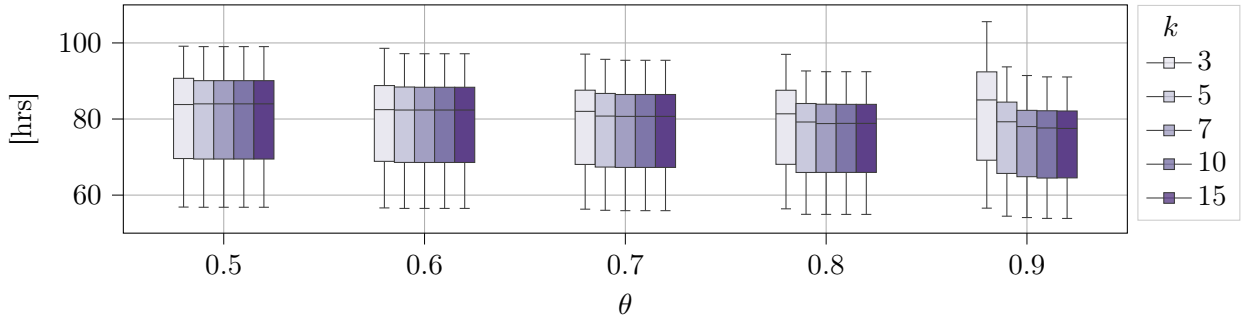


Figure 10: Total delay in the RDUO for various combinations of k and θ .

To illustrate the visual differences among alternative route configurations, Figure 11 presents examples of route variations for both a long and a short trip under various parameter settings. High values of k combined with low θ generate routes excessively long in distance, which frequently must be discarded due to violating the latest arrival constraints even under free-flow conditions. Conversely, configurations with low k and high θ produce highly similar routes that cover limited network areas, complicating effective traffic distribution. Optimal choices thus generally fall into two categories: either low k with low θ , or high k with high θ . Although higher values may achieve more comprehensive network coverage, we select the smaller parameter combination ($k = 5, \theta = 0.6$) to substantially reduce computational complexity while maintaining sufficient route diversity.

Appendix E Detailed instances description

In this section, we provide a detailed overview of the characteristics of the instances under consideration. Figure 12 illustrates various key attributes of these instances aggregated together. The free-flow travel time for the routes ranges from approximately 3 to 15 minutes, including alternative route options. The relative maximum detour, defined as the percentage increase in free-flow travel time between the shortest and longest (in distance) available route for a given trip, most frequently centers around 25%, although in some cases the longest route covers twice the distance of the short-

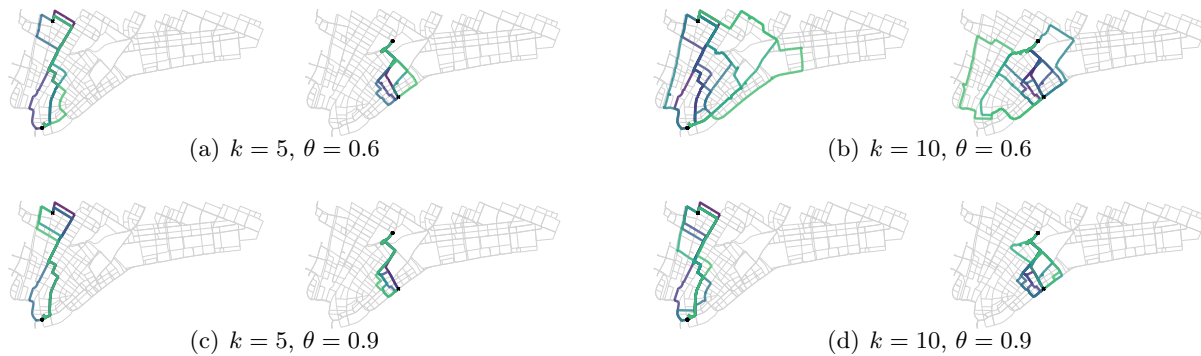


Figure 11: Alternative routes for a long and a short trip with different k and θ values.

est. Most trips have a service time window between six and twelve minutes, with a few extending up to twenty minutes. Lastly, most trips allow for a maximum staggering period of roughly one minute, with a few cases extending up to three minutes. Table 1 summarizes the main characteristics of the RDUO solution for each day considered. For each day, we report the number of trips $|\mathcal{R}|$, the total travel time Z , the total delay D in the RDUO and their ratio, as well as statistics related to the delay experienced by individual trips d^r and the ratio between their actual travel time $\tau^r(r)$ and the corresponding free-flow travel time $\bar{\tau}^r(r)$. On average, the instances contain approximately 6000 trips, and the RDUO total delay accounts for roughly 12% of the total travel time. The individual trip delays pass basic sanity checks: no trip experiences more than four minutes of delay, and travel times never exceed twice the corresponding free-flow travel time.

Appendix F Parameter sensitivity analysis of the LNS

To evaluate the impact of parameter settings on the performance of the LNS algorithm, we conduct a sensitivity analysis by varying three key parameters: the initial pool size x , the sample size y drawn from the pool, and the number of destroy-repair cycles z performed before invoking the local search for intensification. Figure 13 presents heatmaps illustrating how different combinations of these parameters affect total delay reduction across five representative days—specifically, days 27 to 31 of the instances described in Appendix E. We also report the average delay reductions across these days. Each run is subject to a time limit of three hours.

First, increasing the number of destroy-repair cycles z tends to slow down the algorithm and may reduce its effectiveness, with the highest delay reductions often observed between $z = 2$ and $z = 4$. This suggests that it is more advantageous to intensify early using local search and then rebuild a new pool of trips, rather than repeatedly destroying and repairing the same set. Second, a moderate initial pool size, especially $x = 30\%$ or 40% , tends to give better results in most settings. Starting from $x = 50\%$, we generally observe a drop in performance. A larger pool appears beneficial as it includes both highly congested trips - prime candidates for improvement - and less congested ones, thereby supporting more effective exploration of the solution space.

Table 1: Summary of RDUO characteristics for the instances considered. We report the day, the number of trips $|\mathcal{R}|$, the total travel time Z , the total delay D , their ratio, and the average, median, and maximum values of the total delay per trip d^r . We also include the corresponding statistics for the ratio between each trip’s travel time and its free-flow travel time (with a value of 1 indicating free-flow conditions).

Day	$ \mathcal{R} $	Z [hrs]	D [hrs]	Z/D [%]	d^r [min]			$\tau^r(r)/T^r(r)$		
					Avg	Med	Max	Avg	Med	Max
1	5283	561	54	9.63	0.65	0.55	2.90	1.11	1.09	1.62
2	5428	578	60	10.38	0.70	0.56	2.77	1.12	1.10	1.59
3	5557	598	64	10.70	0.73	0.59	3.60	1.12	1.10	1.68
4	5448	575	56	9.74	0.65	0.55	2.80	1.11	1.09	1.55
5	5399	575	57	9.91	0.67	0.58	2.78	1.11	1.10	1.54
6	6309	689	81	11.76	0.81	0.69	3.18	1.14	1.11	1.70
7	5857	626	70	11.18	0.76	0.65	3.04	1.13	1.11	1.68
8	5937	635	70	11.02	0.75	0.63	3.00	1.13	1.11	1.61
9	6325	690	83	12.03	0.83	0.72	3.45	1.14	1.12	1.70
10	5807	628	67	10.67	0.73	0.62	2.97	1.12	1.10	1.83
11	5574	599	62	10.35	0.71	0.60	2.96	1.12	1.10	1.50
12	6142	656	72	10.98	0.75	0.64	3.12	1.13	1.11	1.57
13	6572	715	88	12.31	0.85	0.74	3.14	1.14	1.12	1.71
14	6275	675	78	11.56	0.79	0.67	3.52	1.13	1.11	1.82
15	6281	679	81	11.93	0.82	0.69	3.33	1.14	1.12	1.83
16	6627	725	90	12.41	0.86	0.73	3.64	1.14	1.12	1.76
17	6344	688	83	12.06	0.84	0.68	3.37	1.14	1.12	1.85
18	5747	624	69	11.06	0.75	0.63	3.04	1.12	1.11	1.61
19	5611	603	63	10.45	0.71	0.61	3.59	1.12	1.10	1.59
20	6478	708	85	12.01	0.84	0.71	3.09	1.14	1.12	1.87
21	6622	722	90	12.47	0.87	0.75	3.54	1.15	1.13	1.78
22	6194	673	76	11.29	0.78	0.68	3.02	1.13	1.11	1.65
23	6471	707	88	12.45	0.86	0.72	3.38	1.14	1.12	1.82
24	6109	668	78	11.68	0.81	0.67	3.31	1.13	1.11	1.67
25	5355	573	58	10.12	0.68	0.56	3.22	1.11	1.10	1.54
26	6240	673	79	11.74	0.80	0.67	3.56	1.14	1.11	1.96
27	6593	722	88	12.19	0.85	0.72	3.56	1.14	1.12	1.71
28	6443	698	84	12.03	0.84	0.70	3.59	1.14	1.12	1.72
29	6353	680	79	11.62	0.79	0.67	3.07	1.14	1.11	1.64
30	6715	736	92	12.50	0.87	0.74	3.82	1.15	1.13	1.90
31	6144	680	81	11.91	0.84	0.68	3.60	1.14	1.11	1.64
Avg	6072	657	76	11.57	0.78	0.66	3.26	1.13	1.11	1.70

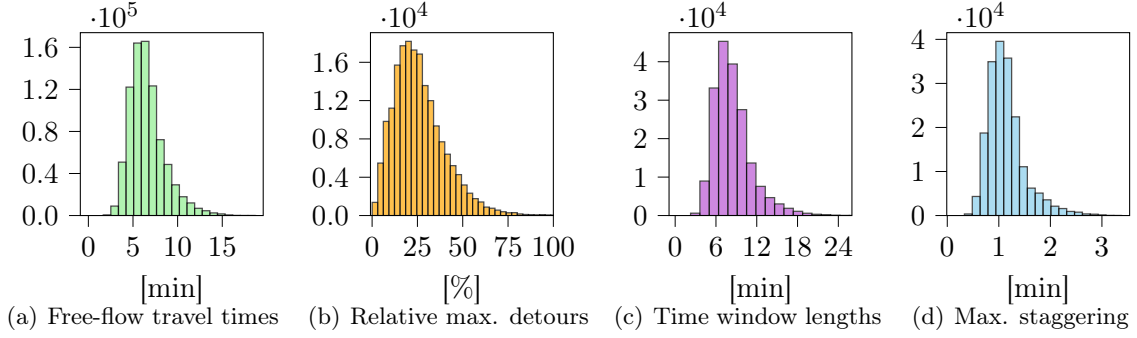


Figure 12: Frequency histograms summarizing key trip features across all instances: (a) free-flow travel times, (b) relative maximum detours between shortest and longest assigned routes, (c) lengths of time windows, and (d) maximum staggering allowed per trip.

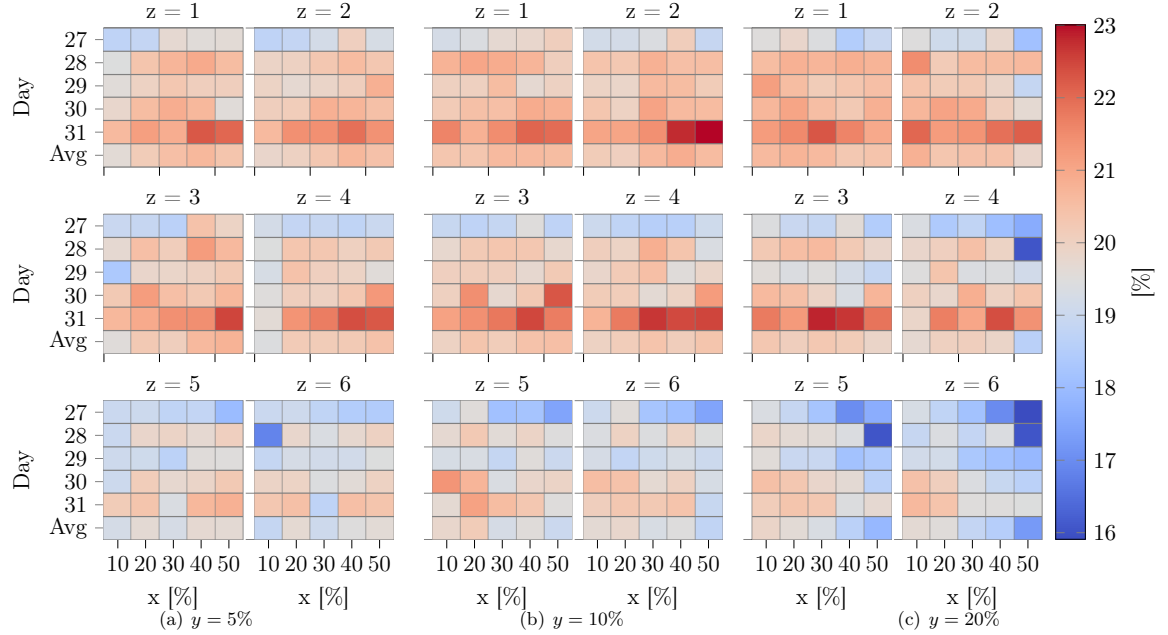


Figure 13: Total delay reduction across five representative days and averaged values for different parameter configurations of the LNS. We vary the initial pool size $x\%$, the sample size $y\%$ drawn from the pool, and the maximum number of destroy-repair cycles z performed before invoking the local search operator for intensification.

Regarding the sample size y , the configuration with $y = 10\%$ offers the most robust performance, achieving high average delay reductions with relatively low variability across days. In contrast, sample sizes of $y = 5\%$ and $y = 20\%$ lead to greater variability and more frequent underperformance. This suggests that while the sampling procedure is helpful, once a promising pool of trips has been identified, it is more effective to focus on optimizing a moderately sized subset of trips rather than attempting to destroy and reinsert larger portions at once.

Appendix G Experimental setup for the STAG and MATH comparison

This appendix describes the experimental setup used to compare the staggering-only variant of our algorithm, STAG, with the matheuristic MATH developed for the same problem.

We run the experiments on the full Manhattan network, preprocessed with contraction hierarchies using a maximum shortcut length of 500 meters (cf. Geisberger et al. 2008), and compute nominal travel times assuming a constant speed of 20 km/h. We extract trip origins, destinations, and earliest departure times from the NYC taxi dataset collected in January 2015. We construct 31 instances, each consisting of 5000 trips sampled between 4:00 and 5:00 p.m. on a different day of the month. As a baseline, we simulate an uncontrolled scenario in which each trip departs as early as possible and follows the shortest-distance route. To model congestion, we define arc travel times using piecewise linear functions:

$$\tau_a^r = \tau_a + \max_{k \in K} \left\{ 0, \sum_{1 \leq k' \leq k} \mu_a^{k'} \cdot (f_a^r - \hat{f}_a^{k'}) \right\},$$

where $\tau_a > 0$, $\mu_a^k > 0$, $\hat{f}_a^k > 0$, and $K = 3$ denotes the number of non-flat segments. We control traffic intensity by restricting arc capacities to allow one AMoD trip every 15 seconds. Accordingly, we set the first breakpoint to $\hat{f}_a^1 = \lceil \tau_a / 15 \rceil$, and define the remaining breakpoints as $\hat{f}_a^2 = 2 \cdot \hat{f}_a^1$ and $\hat{f}_a^3 = 3 \cdot \hat{f}_a^1$. The corresponding slopes are:

$$\mu_a^1 = \frac{0.5 \cdot \tau_a}{\hat{f}_a^1}, \quad \mu_a^2 = \frac{\tau_a}{\hat{f}_a^1}, \quad \mu_a^3 = \frac{1.5 \cdot \tau_a}{\hat{f}_a^1}.$$

Under the chosen parameter configuration, total delays in the baseline setting span from two to thirty hours, with a median of approximately six hours. To explore the impact of departure-time flexibility, we generate two sets of instances — $\bar{\sigma} \downarrow$ and $\bar{\sigma} \uparrow$ — by setting the maximum allowable start time shift $\bar{\sigma}^r$ to 10% and 20% of the nominal travel time along each trip’s assigned route, respectively. The latest arrival time ℓ^r allows for a maximum travel time equal to 125% of the free-flow time of the assigned route.

To conclude, we configure STAG with parameters $x = 50\%$, $y = 10\%$, and $z = 25$, chosen via a calibration procedure similar to that described in Appendix F. For MATH, we set a time limit of two hours. Further implementation details are available at https://github.com/tumBAIS/integ_bal_stag.